

Flocking of Unmanned Aerial Vehicles under Visual Relative Positioning

by

Xiyuan Liu

A Thesis Submitted to
The Hong Kong University of Science and Technology
in Partial Fulfillment of the Requirements for
the Degree of Master of Philosophy
in the Department of Electronic and Computer Engineering

August 2019, Hong Kong

Authorization

I hereby declare that I am the sole author of the thesis.

I authorize the Hong Kong University of Science and Technology to lend this thesis to other institutions or individuals for the purpose of scholarly research.

I further authorize the Hong Kong University of Science and Technology to reproduce the thesis by photocopying or by other means, in total or in part, at the request of other institutions or individuals for the purpose of scholarly research.

Xiyuan Liu

August 2019

Flocking of Unmanned Aerial Vehicles under Visual Relative Positioning

by

Xiyuan Liu

This is to certify that I have examined the above MPhil thesis
and have found that it is complete and satisfactory in all respects,
and that any and all revisions required by
the thesis examination committee have been made.

Prof. Li Qiu, Thesis Supervisor

Prof. Bertram Emil Shi, Department Head

Thesis Examination Committee

1. Prof. Shaojie Shen (Chairperson) Department of Electronic and Computer Engineering
2. Prof. Li Qiu (Supervisor) Department of Electronic and Computer Engineering
3. Prof. Wei Chen Department of Electronic and Computer Engineering

Department of Electronic and Computer Engineering
August 2019

Acknowledgments

I would never have completed this work without the help from many people. First of all, I thank my supervisor, Prof. Li Qiu, for his continuous support and guidance in the process of my MPhil study at HKUST and for his motivation and patience in my diffident times.

I thank the members of my thesis committee, Prof. Wei Chen, for his constructive criticism and suggestions through every group meetings and Prof. Shaojie Shen, for his inspiration and assistance in the area of unmanned aerial vehicles during my graduate studies and their insightful comments on improving this work.

I thank Prof. Jiugang Dong from HIT for his personal guidance along the work on mathematical models. I thank all my colleagues for assisting me in academic researches and organizing colorful events to release my pressure and enjoy my life. I thank Fei Gao and Luqi Wang for their practical skills in conducting UAV experiments and Yifei Shi for helping me setup the flocking environment.

Last but not least, I thank my parents and my girlfriend Xin Mao, for their mental and spiritual support and encouragement through my graduate study, especially during the difficult times.

TABLE OF CONTENTS

Title Page	i
Authorization Page	ii
Signature Page	iii
Acknowledgments	iv
Table of Contents	v
List of Figures	vii
List of Tables	viii
Abstract	ix
Chapter 1 Introduction	1
Chapter 2 Preliminaries and Related Work	5
2.1 Fixed Topology	5
2.1.1 Second-Order System	5
2.1.2 First-Order System	7
2.2 Dynamic Topology	8
Chapter 3 Design of Control Model	9
3.1 Proposed Control Law	9
3.2 Proof of Cohesion and Separation	11
3.3 Proof of Velocity Convergence	13
Chapter 4 Implementation on UAVs	15
4.1 UAV Model	15
4.1.1 Coordinate Frame	15
4.1.2 UAV Dynamics and Kinematics	16
4.2 Hardware architecture	18
4.3 Software architecture	20
Chapter 5 Experiments and Evaluation	23
5.1 Simulation of Flocking Models	23
5.2 Comparison with Formation Algorithm	30
5.2.1 Formation Performance	31
5.3 Realization of Proposed Model	32
5.3.1 Indoor Environment	32
5.3.2 Outdoor Environment	32

Chapter 6 Conclusion **36**

References **37**

LIST OF FIGURES

1.1	Flocking of two UAVs in GPS-denied environments. A video of the experiments can be found at https://youtu.be/lIJ_8VM-yS0 .	3
1.2	Our complete flocking system: the left one (leader) is manually controlled and the right one (follower) is fully autonomous.	4
2.1	Examples of $\alpha_{ij}(x)$ in [10], $f(x)$ in [8] and $V_{ij}(x)$ in [36].	6
2.2	Examples of dynamic topology and modified potential function.	8
3.1	Examples of $f_0(x), f_1(x)$ in (3.1).	10
4.1	Coordinate frames of world, UAV body and on-board camera.	15
4.2	Nested control loops for position and attitude control, [22].	17
4.3	Follower UAV and remote controller panel: (1) Lightbridge 2 receiver; (2) Intel NUC mini computer; (3) Intel Realsense camera; (4) 4S LiPo Batter Case; (5) DJI snail motor; (6) iPad Live streaming panel; (7) DJI Lightbridge 2 remote controller; (8) DJI N3 flight controller.	18
4.4	Leader UAV.	19
4.5	On-board power systems.	20
4.6	Software architecture.	21
5.1	Averaged ψ_{angle} of twenty simulations of two agents w.r.t various σ, β . Their initial velocities are all randomized and nonzero.	24
5.2	Average ψ_{angle} and relative distance of multiple agents with fixed $\sigma = 1$ and $\beta = 0.25$. Their initial velocity are all randomized and nonzero.	25
5.3	Initial position settings of multi-agent flocking simulations in MATLAB.	25
5.4	Convergence descriptors ψ_{angle} of model 1 ([42]), 2 ([10]), 3 ([8]) and our proposed one.	26
5.5	Magnitudes of agents' velocities of model 1 ([42]), 2 ([10]), 3 ([8]) and our proposed one.	27
5.6	Average relative distances between neighboring agents. The blue and red dashed line indicate two boundaries ($d_0^{\frac{1}{2}}, d_1^{\frac{1}{2}}$) in our proposed model. Model 1, 2 and 3 are from [42], [10] and [8] respectively.	28
5.7	Motion simulations with initial velocities whose directions and magnitudes are indicated by corresponding arrows.	29
5.8	Formation algorithm in [6].	30
5.9	Plots of tracking algorithm.	31
5.10	Flocking in x-axis.	33
5.11	Flocking in y-axis.	34
5.12	Flocking in xy-plane.	35

LIST OF TABLES

- | | |
|---|----|
| 4.1 Weight and power consumption of components on the follower UAV. | 18 |
|---|----|

Flocking of Unmanned Aerial Vehicles under Visual Relative Positioning

by Xiyuan Liu

Department of Electronic and Computer Engineering

The Hong Kong University of Science and Technology

Abstract

In the past few decades, researchers have been studying the motion pattern of bird flocks, learning from biomimetics and imitating their behaviors with small scale mobile robots due to its potential applications in those environments where self-organizing, healing and configuring capabilities are desired. Various control laws have been developed for mass particles and verified with simulation results, however, few of them have been implemented on real unmanned aerial vehicles (UAVs). On the flip side, existing UAV flockings rely heavily on centralized control or measurement, which fail to percept and determine their individual movement like natural birds. This leaves us an empty space worthwhile to discover: the realization of UAV flockings with distributed control algorithms.

In this thesis, we first review flocking related consensus problems, propose a second-order multi-agent system and prove its stability. Second, we present the design of our flocking system: one manually controlled leader UAV and one autonomous driving follower UAV with 1.12 kg total weight, 25 cm diagonal length and the monocular camera as the only on-board sensor. Last but not least, simulations, comparison with the traditional tracking algorithm and experiments in both indoor and outdoor GPS-denied environments are demonstrated. It is shown that our solution converges as fast as C-S model, enjoys shorter relative distance than C-D model and reacts faster than tracking algorithm.

CHAPTER 1

INTRODUCTION

Bird flocking is a natural phenomenon which always appears in group activities like collective hunting, entertainment or migration. Biologists have found that the flocking behavior benefits the entire colony by improving the overall foraging [28], predators spotting [4] and propagation [18] efficiencies. Specifically, the allocation of individual tasks, communication and motion control of each agent have determined the main characteristics of the flock system, such as the scalability, robustness and convergence rate. Missions like remote transportation, surveillance and rescue with UAVs require the agents to be fully autonomous, fault tolerant and intelligent that they could dynamically interact with the environments and local neighbors. Studies regarding the motion control and the realization of flocking with mobile robots will greatly inspire the human beings on resolving the aforementioned tasks.

Three important criteria were first studied in [32] to determine a stable flocking system: separation, cohesion and alignment. Alignment criterion requires each agent to match self's velocity with neighboring flockmates in the mid range, separation criterion requires each agent to repel neighboring flockmates in the short range and cohesion criterion requires each agent to steer neighboring flockmates in the long range. ψ_{angle} (1.1) is defined to describe the convergence of agents' velocities in angle, where k is the total number of agents and ψ_{angle} goes to one when all agents' velocities converge to a common direction.

$$\psi_{\text{angle}}(t) = \frac{1}{k(k-1)} \sum_{i=1}^k \sum_{j \neq i} \frac{v_i(t)v_j(t)}{|v_i(t)||v_j(t)|} \quad (1.1)$$

To better control the individual agents and realize the flocking system, quadrotors or UAVs are selected owing to their flexibility and mobility in 3D space. Today, the capability of a single UAV has been increasing rapidly, accompanied by the falling prices and improving performance of the communication, sensing and processing hardwares.

Meanwhile, the measurement and control methods of UAVs in the flock realization are expected to be distributed. Realization with distributed measurement method requires all the information to be collected by on-board sensors, such as LiDAR, inertial measurement unit (IMU) or camera instead of external absolute positioning systems like GPS [41], motion capture system (VICON) [7, 2] or real-time kinematic system (RTK). Realization with distributed control method requires each UAV to decide its movement with information available at that agent [5] instead of executing commands from a central computer [40, 27, 43] or a leader UAV. The assumption of distributed architectures agrees with the nature that individual agents react to their sensed local environment and surrounding neighbors.

UAV formations [31, 24, 34, 1, 39, 11] are often discussed with flockings [44, 35, 41, 19, 14] since their cluster-like performances are very similar, however, they are distinct in several aspects. The formation problem emphasizes the relative positions [31, 24, 34], displacements [1, 39] or distances [11] between any two agents to be fixed, while the flocking problem focuses more on the coordination of all agents instead of preserving a rigid shape. The flocking model's fault tolerance ability outperforms that of formation model. The adding or removing one agent from the flocking model will not affect its stability, however, the formation will not exist if one agent is removed. From application side, the control and measurement methods of formation problems are mostly centralized and for agents in the formation model, their final stable states are independent of their initial conditions. On the contrary, the control and measurement methods of flocking problems are expected to be distributed and the final stable states of agents in flocking model depend on the initial conditions.

The gap between the simulation and the realization of the flocking models comes from two sides, the design of the model and the design of the UAV platform. From the theoretical side, first, the convergence rate of agents' velocities in flocking model is expected to be fast to prevent collisions between agents. Second, the inter-agent distance of any two agents in stable state shall live within an appropriate range that the lower and upper bounds have to be addressed due to safety and sensors' limited operating range reasons. Third, the control algorithm has to be distributed that only relative information could be used. From the experimental side, first, the control and measurement methods have to be

distributed that each UAV could only use on-board sensors to percept the local environment, analyse and make decisions instead of relying on external sensors (indoor motion capture system or outdoor GPS) or centralized computer. Second, the on-board sensor is capable of measuring relative displacements. Third, camera is preferred to be the on-board sensor to maximally imitate natural birds.



Figure 1.1. Flocking of two UAVs in GPS-denied environments. A video of the experiments can be found at https://youtu.be/IJj_8VM-yS0.

In this thesis, we present a complete system-level solution to address the aforementioned challenges. The theoretical contribution is the proposal and the proof of a control law satisfying the three flocking criteria. The application-level contribution is the design, control and the implementation of the control law using two UAVs, with the front one being controlled manually and the latter one being fully autonomous as shown in Fig. 1.1 and Fig. 1.2. We use the monocular camera as our only on-board sensor for both state estimation and target recognition to maximally imitate natural birds. The flight tests are conducted in both indoor and outdoor environments, and it is successfully demonstrated that our autonomous UAV is able to stay flocking with the proposed control law.



Figure 1.2. Our complete flocking system: the left one (leader) is manually controlled and the right one (follower) is fully autonomous.

The outline of the thesis is as follows, Ch. 2 reviews the origin and some typical approaches of the flocking related consensus problem. Our proposed control model and its stability and convergence analysis are shown in Ch. 3. Ch. 4 discusses the architecture and the implementation of our hardware and software platforms. Simulations and real world experiments are demonstrated in Ch. 5. Ch. 6 summarises this work and points out our possible improvements and future plans.

CHAPTER 2

PRELIMINARIES AND RELATED WORK

2.1 Fixed Topology

2.1.1 Second-Order System

Bird flocking or distributed behavior model was first studied in [32] to animate the aggregate motion of birds in computer simulation. Based on [32] and observations, a discrete time model (2.1) and the correlation between flock coherence and particle density have been discussed in [42]. In this model, each particle has a constant velocity, while its direction is determined by $\langle \theta(t) \rangle_r$, which is the average direction of the neighboring particles within radius r , with $\Delta\theta$ representing the random noise. To clarify the notation, we identify the set of k agents as $V = \{1, \dots, k\}$ and $x_{ij} = x_i - x_j$, where x_i or $x_i(t)$ and v_i or $v_i(t) \in \mathbb{R}^n$ represent the position and velocity of agent i at time t respectively. Unless otherwise noted, we assume the initial positions of the agents are distinct that $x_i(0) \neq x_j(0)$ for $i, j \in V$.

$$\begin{aligned} x_i(t + \Delta t) &= x_i(t) + v_i(t)\Delta t \\ \theta(t + \Delta t) &= \langle \theta(t) \rangle_r + \Delta\theta \end{aligned} \tag{2.1}$$

In [17], the convergence of the model (without noise) in [42] is proved, however, neither the speeds of birds in nature are constant, nor the headings of birds can be drastically changed that (2.1) cannot be applied for realization. [10] has proposed a control law (2.2, Fig. 2.1(a)) to resolve the velocity alignment and cohesion problem that the convergence of the flock to a common velocity is guaranteed, however, collision avoidance between agents cannot be assured. Similar protocols including communication delay have been summarized in [23, 30]. The weight $a_{ij}(x) : \mathbb{E}^k \rightarrow [0, \infty)$ qualifies the influence of agent j acting on agent i , which is a function of agent positions. In [42], $a_{ij}(x)$ could be equally defined as (2.3).

$$\ddot{x}_i(t) = \sum_{j=1}^k a_{ij}(x)(v_j - v_i) \quad (2.2)$$

$$a_{ij}(x) = \frac{K}{(\sigma^2 + \|x_i - x_j\|^2)^\beta}$$

$$a_{ij}(x) = \begin{cases} 1, & \text{if } \|x_i - x_j\| \leq r \\ 0, & \text{otherwise} \end{cases} \quad (2.3)$$

Based on [10], [8] has further proved the separation of the flocks that the relative distance between each pair of agents will always be greater than a certain lower bound, by appending a collision avoidance term (2.4). $f(\cdot)$ is a repelling function, $\Lambda(\cdot)$ is a regulating factor and the definition of $a_{ij}(x)$ remains the same as (2.2). An example of $f(x) = \frac{1}{(x-d_0)^\theta}$ is illustrated in Fig. 2.1(b).

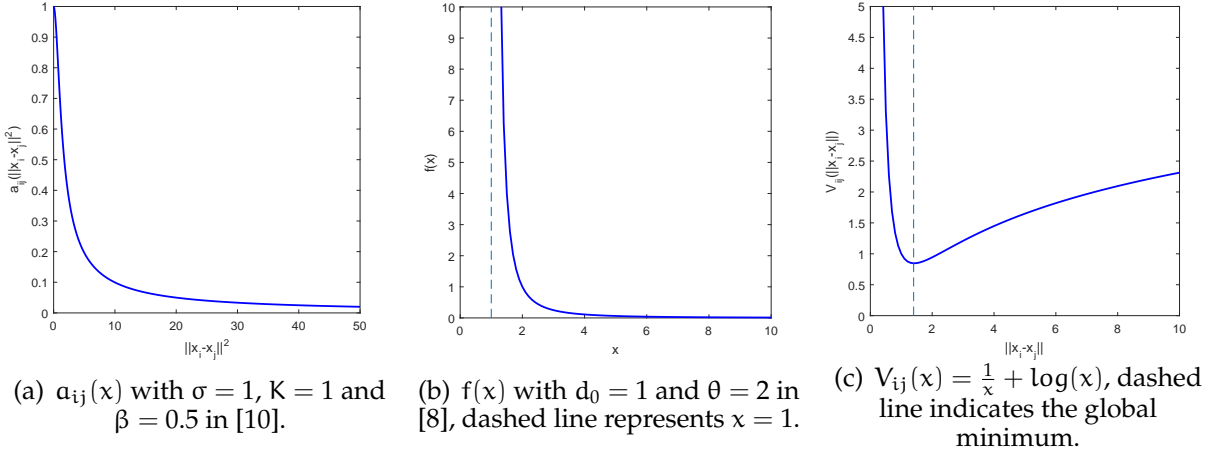


Figure 2.1. Examples of $a_{ij}(x)$ in [10], $f(x)$ in [8] and $V_{ij}(x)$ in [36].

$$\ddot{x}_i(t) = \underbrace{\sum_{j=1}^k a_{ij}(x)(v_j - v_i)}_{\text{velocity consensus term}} + \underbrace{\Lambda(v) \sum_{j \neq i} f(\|x_i - x_j\|^2)(x_i - x_j)}_{\text{collision avoidance term}} \quad (2.4)$$

$$\Lambda(v) = \left(\frac{1}{k} \sum_{i>j} \|v_i - v_j\|^2 \right)^{\frac{1}{2}}$$

Gradient-based schemes (2.5) have also been developed in [36, 25, 38, 26] to stabilize

inter-agent distances. With the designed artificial potential function $V_{ij}(x)$ (Fig. 2.1(c)) in [36], the relative distance between agents is expected to locate at the unique minimum. In [25], three flocking rules from [32], split, rejoin and squeeze maneuvers have been embodied within their proposed model (2.6), where $\phi(\cdot)$ is a potential function, n_{ij} is the unit vector along the line connecting x_i and x_j and a_{ij} denotes corresponding adjacency matrix element. When the total number of agents is greater than ten, however, fragmentation may occur that a collective reference pair (x_r, v_r) has to be introduced.

$$\ddot{x}_i(t) = \underbrace{\sum_{j \in V} (v_j - v_i)}_{\text{velocity consensus term}} + \underbrace{\left(-\sum_{j \in V} \nabla_{x_i} V_{ij} \right)}_{\text{gradient-based term}} \quad (2.5)$$

$$\ddot{x}_i(t) = \underbrace{\sum_{j \in V} a_{ij}(x)(v_j - v_i)}_{\text{velocity consensus term}} + \underbrace{\sum_{j \in V} \phi(\|x_j - x_i\|_\sigma) n_{ij}}_{\text{gradient-based term}} + \underbrace{(-c_1(x_i - x_r) - c_2(v_i - v_r))}_{\text{navigational feedback term}} \quad (2.6)$$

2.1.2 First-Order System

In [15] (2.7), [12] (2.8) and [13] (2.9), first-order control models have been studied that with carefully designed attraction and repulsion functions, Lyapunov function candidates and LaSalle's Invariant Principle, all the flock members are expected to converge to a constant arrangement ($\dot{x} = 0$) within a hyper-ball. Separation is ensured in the first-order system, however, velocity alignment is less satisfied.

$$\dot{x}_i = \sum_{j=1}^N (1 - e^{-\|x_i - x_j\|^2})(x_j - x_i) \quad (2.7)$$

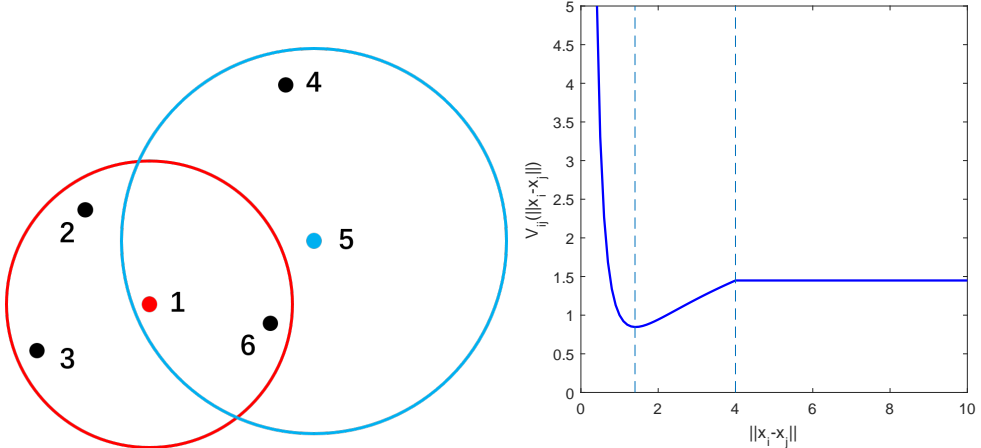
$$\dot{x}_i = - \sum_{j \in V} \frac{\partial W_{ij}}{\partial x_i} - \sum_{j \in V} \frac{\partial V_{ij}}{\partial x_i} \quad (2.8)$$

$$\dot{x}_i = \sum_{j \in V} \frac{2\rho_{ij}}{\gamma_{ij}^2} (D_{ij})_i x \quad (2.9)$$

2.2 Dynamic Topology

Unlike above mentioned theories assume, [3] discovered that interaction between agents in flocking does not necessarily depend on the metric distance but rather on the topological distance. An average number of six to seven nearest neighbors are involved in the interaction instead of the whole neighbors within a fixed distance. An example is illustrated in Fig. 2.2(a), where the number of nearest neighbors involved, denoted by q , is three and the total number of agents, denoted by k , is six. Given conditional initial positions, velocities and original a_{ij} in (2.3), [20] has proved that the agents asymptotically agree on a common velocity. Based on [20], [9] have further introduced the quotient $\frac{q}{k-1}$ that unconditional flocking occurs when $\frac{q}{k-1} \geq \frac{1}{2}$.

In [37], it is shown that with modified potential function (Fig. 2.2(b)), where the potential is constant when the relative distance between two agents is larger than a certain limit and original control model (2.5), the stability of the flock is guaranteed if no agent is separated initially.



(a) A flock of agents with $q = 3$, $k = 6$, three closest neighbors of agent 1 and agent 5 are agents 2, 3 and 6 and agents 1, 4 and 6 respectively.

(b) V_{ij} in [37]. The left dashed line indicates the global minimum and the right dashed line indicates a interaction range. The disconnection of the potential function does not affect the stability.

Figure 2.2. Examples of dynamic topology and modified potential function.

CHAPTER 3

DESIGN OF CONTROL MODEL

3.1 Proposed Control Law

Considering a flock of k agents whose behaviors are described by (3.1, 3.2) in continuous time with initial positions satisfying $d_0 < \|x_i(0) - x_j(0)\|^2 < d_1$ for all $i \neq j$. At every time step t , all agents update their states with the information of the relative displacements and velocities between themselves and their neighboring agents. Compared with [8], a cohesion term is appended to the u_i for the purpose of faster convergence and a more compact cohesion. We prove that when $\beta \leq \frac{1}{2}$, the velocities of agents in the flock will converge to a common value without collision with others. The regulator $\Lambda(v)$ is designed to adjust the internal repulsion and attraction forces from neighboring agents. Examples of $f_0(x)$, $f_1(x)$ are illustrated in Fig. 3.1.

$$\dot{x}_i(t) = v_i(t)$$

$$\dot{v}_i(t) = u_i(t)$$

$$\begin{aligned}
u_i(t) = & \underbrace{\sum_{j=1}^k a_{ij}(x)(v_j - v_i)}_{\text{alignment term}} + \\
& \underbrace{\Lambda(v) \sum_{j \neq i} f_0(\|x_i - x_j\|^2)(x_i - x_j)}_{\text{separation term}} + \\
& \underbrace{\Lambda(v) \sum_{j \neq i} f_1(\|x_i - x_j\|^2)(x_j - x_i)}_{\text{cohesion term}}
\end{aligned} \tag{3.1}$$

$$\begin{aligned}
a_{ij}(x) &= \frac{K}{(\sigma^2 + \|x_i - x_j\|^2)^\beta} \\
\Lambda(v) &= \left(\frac{1}{k} \sum_{i>j} \|v_i - v_j\|^2 \right)^{\frac{1}{2}} \\
f_0(x) &= \frac{1}{(x - d_0)^\theta} \\
f_1(x) &= \frac{1}{(x - d_1)^\theta}
\end{aligned} \tag{3.2}$$

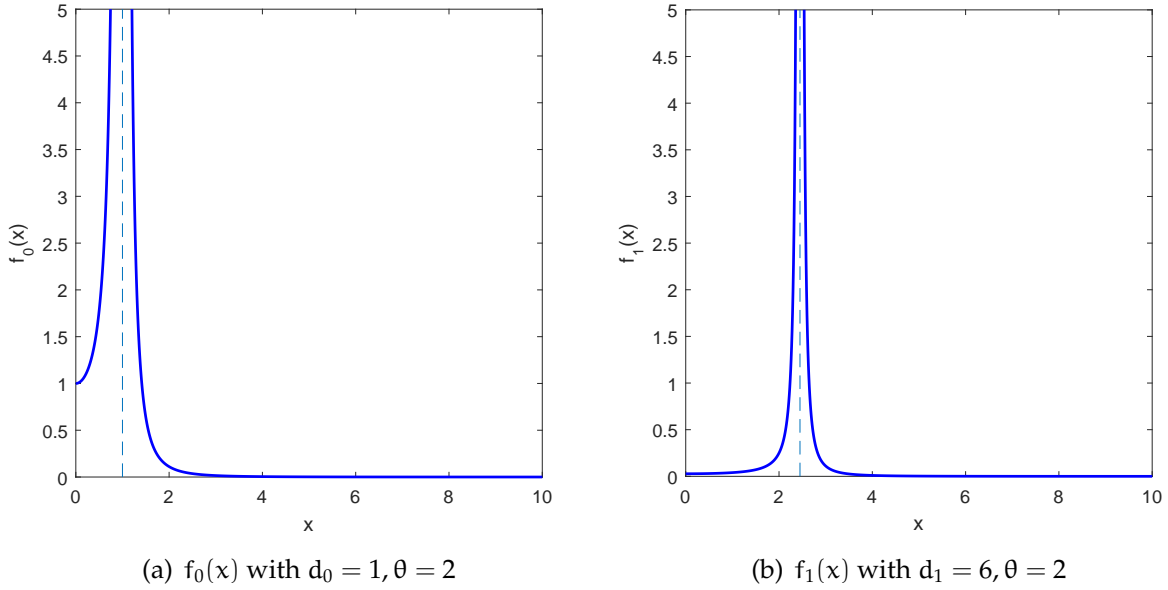


Figure 3.1. Examples of $f_0(x), f_1(x)$ in (3.1).

In this flocking model, all agents are treated homogeneously that we assume each agent is identical in terms of size, mass or kinematics (3.3). For heterogeneous agents still governed by second-order dynamics with various physical characteristics, modifications in the transfer function may possible resolve this issues (3.4), where $\frac{k_1}{s}$ and k_2 represent various properties of heterogeneous agents, x and u denote the positions and control input (acceleration) respectively, and we leave this as our future works.

$$\frac{1}{s^2} = \frac{x}{u} \tag{3.3}$$

$$\frac{1}{s^2} + \frac{k_1}{s} + k_2 = \frac{\mathbf{x}}{\mathbf{u}} \quad (3.4)$$

3.2 Proof of Cohesion and Separation

Here we omit the detailed proofs of the Lemmas and Propositions originated from [8]. Let F_f be the k by k adjacency matrix with entries $f_{ij} = f_0(\|x_i - x_j\|^2) - f_1(\|x_i - x_j\|^2)$ when $i \neq j$ and $f_{ii} = 0$. Let D_f be a diagonal matrix whose entries are $d_{ii} = \sum_{j=1}^k f_{ij}$. We have Laplacian matrix $L_f = D_f - F_f$. Similarly we have $L_x = D_x - A_x$, where a_{ij} is defined in (3.2). Then (3.1) could be equally defined as

$$\begin{aligned} \dot{\mathbf{x}} &= \mathbf{v} \\ \dot{\mathbf{v}} &= -L_x \mathbf{v} + \Lambda(v) L_f \mathbf{x} \end{aligned} \quad (3.5)$$

where $\mathbf{x} = (x_1, x_2, \dots, x_k)^T$ and $\mathbf{v} = (v_1, v_2, \dots, v_k)^T$. Noticed that matrix L_x acts on \mathbb{E}^k by mapping $(v_1, v_2, \dots, v_k)^T$ to $((L_x)_{i1}v_1 + \dots + (L_x)_{ik}v_k)_{i \leq k}$.

Let $\{\Delta = (u, u, \dots, u) | u \in \mathbb{E}\}$ be the diagonal of \mathbb{E}^k , and Δ^\perp be the orthogonal complement of Δ in \mathbb{E}^k . Then we could decompose every element $e \in \mathbb{E}^k = e_\Delta + e^\perp$ with $e_\Delta \in \Delta$ and $e^\perp \in \Delta^\perp$. We then decompose $\mathbf{v} = \mathbf{v}_\Delta + \mathbf{v}^\perp$ where $\mathbf{v}_\Delta = (\bar{v}, \bar{v}, \dots, \bar{v})^T$, $\mathbf{v}^\perp = (v_1 - \bar{v}, \dots, v_k - \bar{v})^T$ and \bar{v} is the average velocity of all k agents. We show that $\langle \mathbf{v}_\Delta, \mathbf{v}^\perp \rangle = \sum_{i=1}^k \langle \bar{v}, v_i - \bar{v} \rangle = \langle \bar{v}, \sum_{i=1}^k (v_i - \bar{v}) \rangle = 0$.

Lemma 1: For any solution $(\mathbf{x}(t), \mathbf{v}(t))$ of (3.5), we have $\frac{d}{dt} \mathbf{v}_\Delta = 0$.

From Lemma 1, we know that \mathbf{v}_Δ is constant with t and $a_{ij}(x) = a_{ij}(x^\perp)$. Thus in the following paragraphs, we use \mathbf{x} and \mathbf{v} to denote \mathbf{x}^\perp and \mathbf{v}^\perp respectively. The system in (3.5) then becomes the following

$$\begin{aligned} \dot{\mathbf{x}} &= \mathbf{v} \\ \dot{\mathbf{v}} &= -L_x \mathbf{v} + \|v\| L_f \mathbf{x} \end{aligned} \quad (3.6)$$

Define the function $E : \mathbb{E}^k \times \mathbb{E}^k \rightarrow (0, \infty)$ by (3.7), where δ is an infinitesimal positive number.

$$\begin{aligned}
E(\mathbf{x}, \mathbf{v}) &= \|\mathbf{v}\| + \frac{1}{2} \sum_{i>j} \int_{\|\mathbf{x}_i - \mathbf{x}_j\|^2}^{d_1 - \delta} f_0(r) dr - \frac{1}{2} \sum_{i>j} \int_{\|\mathbf{x}_i - \mathbf{x}_j\|^2}^{d_1 - \delta} f_1(r) dr \\
&= \|\mathbf{v}\| + \frac{1}{2} \sum_{i>j} \int_{\|\mathbf{x}_i - \mathbf{x}_j\|^2}^{d_1 - \delta} (f_0(r) - f_1(r)) dr
\end{aligned} \tag{3.7}$$

Proposition 1: For all $t > 0$, $-\mathcal{H}k\|\mathbf{v}\| + \langle L_f \mathbf{x}, \mathbf{v} \rangle \leq \frac{d}{dt} \|\mathbf{v}\| \leq -\frac{\mathcal{H}k\|\mathbf{v}\|}{(1+2\|\mathbf{x}\|^2)^\beta} + \langle L_f \mathbf{x}, \mathbf{v} \rangle$.

Lemma 2: Let A be a $k \times k$ positive, symmetric matrix and L be its Laplacian. Then for all $u, w \in \mathbb{E}^k$ (and in particular, for all $u, w \in \Delta^\perp$), $\langle w, Lu \rangle = \sum_{i>j} \langle w_i - w_j, u_i - u_j \rangle a_{ij}$.

Using Proposition 1, Lemma 2 and the fundamental theorem of calculus we see the derivative of E along the solution satisfies

$$\begin{aligned}
\frac{d}{dt} E(\mathbf{x}(t), \mathbf{v}(t)) &= \frac{d}{dt} \|\mathbf{v}(t)\| + \frac{1}{2} \sum_{i>j} \frac{d}{dt} \int_{\|\mathbf{x}_i(t) - \mathbf{x}_j(t)\|^2}^{d_1 - \delta} (f_0(r) - f_1(r)) dr \\
&= \frac{d}{dt} \|\mathbf{v}(t)\| - \frac{1}{2} \sum_{i>j} \frac{d}{dt} \langle \mathbf{x}_i(t) - \mathbf{x}_j(t), \mathbf{x}_i(t) - \mathbf{x}_j(t) \rangle (f_0(\|\mathbf{x}_i(t) - \mathbf{x}_j(t)\|^2) \\
&\quad - f_1(\|\mathbf{x}_i(t) - \mathbf{x}_j(t)\|^2)) \\
&\leq -\frac{\mathcal{H}k}{(1+2\|\mathbf{x}\|^2)^\beta} \|\mathbf{v}\| + \langle L_f \mathbf{x}, \mathbf{v} \rangle - \sum_{i>j} \langle \mathbf{x}_i - \mathbf{x}_j, \mathbf{v}_i - \mathbf{v}_j \rangle (f_0(\|\mathbf{x}_i - \mathbf{x}_j\|^2) \\
&\quad - f_1(\|\mathbf{x}_i - \mathbf{x}_j\|^2)) \\
&= -\frac{\mathcal{H}k}{(1+2\|\mathbf{x}\|^2)^\beta} \|\mathbf{v}\|
\end{aligned} \tag{3.8}$$

Hence $E(\mathbf{x}(t), \mathbf{v}(t))$ is a decreasing function of t along the solution $(\mathbf{x}(t), \mathbf{v}(t))$. Write

$$E(\mathbf{x}(0), \mathbf{v}(0)) = \|\mathbf{v}(0)\| + \frac{1}{2} \sum_{i>j} \int_{\|\mathbf{x}_i(0) - \mathbf{x}_j(0)\|^2}^{d_1 - \delta} (f_0(r) - f_1(r)) dr \tag{3.9}$$

Then for all $t \geq 0$, $E(\mathbf{x}(t), \mathbf{v}(t)) \leq E(\mathbf{x}(0), \mathbf{v}(0))$. This implies

$$\frac{1}{2} \sum_{i>j} \int_{\|x_i - x_j\|^2}^{d_1 - \delta} (f_0(r) - f_1(r)) dr < E(x(0), v(0)) \quad (3.10)$$

From the definition of f_0 and f_1 and the initial conditions that we have ensured $d_0 < \|x_i(t) - x_j(t)\|^2 < d_1$ for all $i \neq j$ and $t \geq 0$, otherwise the integral in (3.7) will go to infinity.

3.3 Proof of Velocity Convergence

Here, we show the proof for the case $\beta \leq \frac{1}{2}$, as the proof for $\beta > \frac{1}{2}$ is similar. From (3.8) we could obtain (3.11, 3.12)

$$E(x(t), v(t)) - E(x(0), v(0)) \leq - \int_0^t \frac{Hk}{(1 + 2\|x(s)\|^2)^\beta} \|v(s)\| ds \quad (3.11)$$

$$\int_0^t \frac{Hk}{(1 + 2\|x(s)\|^2)^\beta} \|v(s)\| ds \leq E(x(0), v(0)) \quad (3.12)$$

Proposition 2: For all $t > 0$, $\frac{d}{dt} \|x(t)\| \leq \|v(t)\|$.

By Proposition 2, we have

$$\frac{d}{dt} \|x(t)\| \leq \|v(t)\| \quad (3.13)$$

$$\int_{\|x(0)\|}^{\|x(t)\|} \frac{Hk}{(1 + 2y^2)^\beta} dy \leq E(x(0), v(0)) \quad (3.14)$$

$$\begin{aligned} E(x(0), v(0)) &\geq \int_{\|x(0)\|}^{\|x(t)\|} \frac{Hk}{(1 + 2y^2)^\beta} dy \geq \int_{\|x(0)\|}^{\|x(t)\|} \frac{Hky}{(1 + 2y^2)^{\beta + \frac{1}{2}}} dy \\ &= \begin{cases} \frac{Hk}{2-4\beta} (1 + 2y^2)^{\frac{1}{2}-\beta} \left| \frac{x(t)}{\|x(0)\|} \right|, & \text{if } \beta \neq \frac{1}{2} \\ \frac{Hk}{4} \ln(1 + 2y^2) \left| \frac{x(t)}{\|x(0)\|} \right|, & \text{if } \beta = \frac{1}{2} \end{cases} \end{aligned} \quad (3.15)$$

Assume $\|\mathbf{x}(t)\|$ is unbounded for $t > 0$, then as $t \rightarrow \infty$, $E(\mathbf{x}(0), \mathbf{v}(0)) \rightarrow \infty$ which contradicts with our initial condition. Thus $\|\mathbf{x}(t)\|$ is bounded which leads to

$$\int_0^\infty \|\mathbf{v}(t)\| dt < \infty \quad (3.16)$$

We show that $\|\mathbf{v}(t)\|$ is a continuous function of t that

$$\begin{aligned} \left| \frac{d}{dt} \|\mathbf{v}(t)\| \right| &\leq Hk \|\mathbf{v}(t)\| + |\langle L_f \mathbf{x}(t), \mathbf{v}(t) \rangle| \\ &= Hk \|\mathbf{v}(t)\| + \left| \sum_{i>j} f(\|\mathbf{x}_i(t) - \mathbf{x}_j(t)\|^2) \langle v_i - v_j, \mathbf{x}_i - \mathbf{x}_j \rangle \right| \\ &\leq Hk \|\mathbf{v}(t)\| + \sum_{i>j} f(\|\mathbf{x}_i(t) - \mathbf{x}_j(t)\|^2) \|v_i - v_j\| \|\mathbf{x}_i - \mathbf{x}_j\| \leq \infty \end{aligned} \quad (3.17)$$

Then we show that when $t \rightarrow \infty$, $\|\mathbf{v}(t)\| \rightarrow 0$. Assumes there exist some $\delta > 0$ that when $t \rightarrow \infty$, $\|\mathbf{v}(t)\| \rightarrow \delta$, then

$$\int_0^\infty \|\mathbf{v}(t)\| dt \geq \infty \quad (3.18)$$

which contradicts (3.16).

CHAPTER 4

IMPLEMENTATION ON UAVS

In this chapter, the UAV's physical model and system architecture is presented, including the software and hardware configurations, specifications of the UAV platform and the details of sensors.

4.1 UAV Model

4.1.1 Coordinate Frame

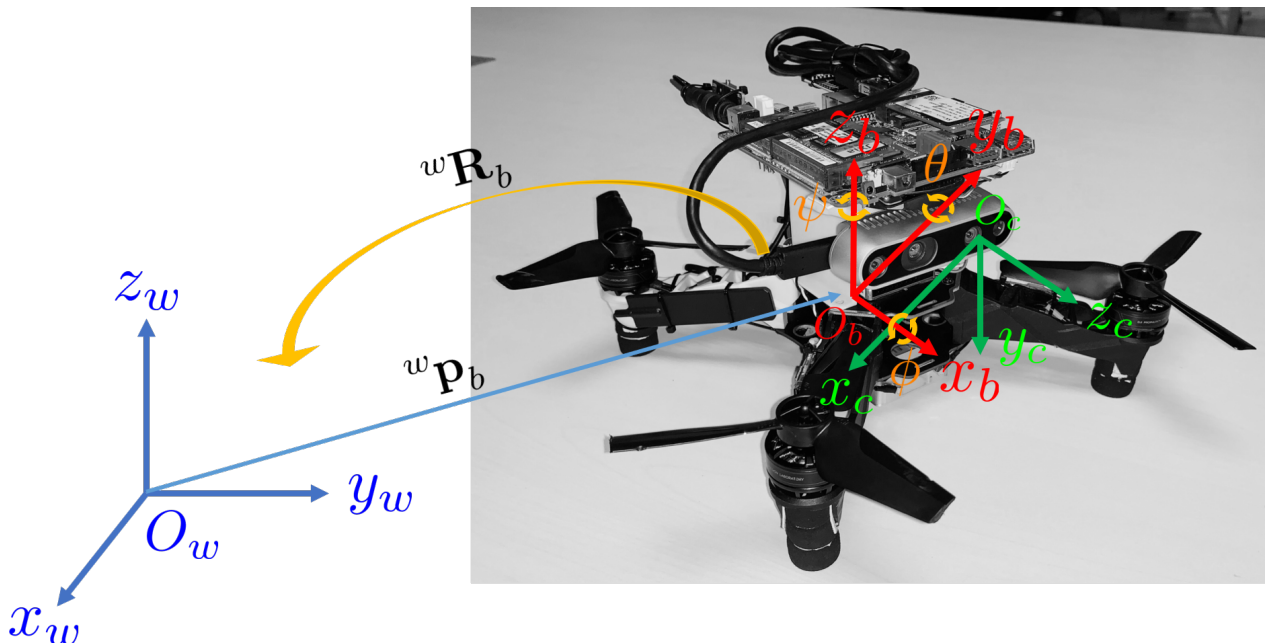


Figure 4.1. Coordinate frames of world, UAV body and on-board camera.

Three coordinate frames are considered in our flocking system including the world, UAV body and on-board camera frames, as illustrated in Fig. 4.1. In Ch. 5.2, the target UAV is first captured in camera frame denoted by $\mathbf{p}_c \in \mathbb{R}^3$, then for the simplicity and unity of the calculations, \mathbf{p}_c is transformed back to world frame $\mathbf{p}_w \in \mathbb{R}^3$ by ${}^w\mathbf{g}_c \in \mathbb{R}^{4 \times 4}$:

$$\begin{aligned}
[\mathbf{p}_w^T \ 1]^T &= {}^w\mathbf{g}_c [\mathbf{p}_c^T \ 1]^T \\
{}^w\mathbf{g}_c &= {}^w\mathbf{g}_b {}^b\mathbf{g}_c = \begin{bmatrix} {}^w\mathbf{R}_b & {}^w\mathbf{p}_b \\ \mathbf{0}^{1 \times 3} & 1 \end{bmatrix} \begin{bmatrix} {}^b\mathbf{R}_c & {}^b\mathbf{p}_c \\ \mathbf{0}^{1 \times 3} & 1 \end{bmatrix} \\
{}^b\mathbf{R}_c &= \mathbf{R}_z(\psi)\mathbf{R}_y(\theta)\mathbf{R}_x(\phi)
\end{aligned} \tag{4.1}$$

where \mathbf{p}_c is first rotated w.r.t z_c by yaw angle ψ , then z_y by pitch angle θ , last z_x by roll angle ϕ and shifted by ${}^b\mathbf{p}_c$ to \mathbf{p}_b in body frame. Iteratively, \mathbf{p}_c is transformed back to \mathbf{p}_w in world frame (4.1). It is worthwhile to point out that both ${}^b\mathbf{g}_c$ and ${}^w\mathbf{g}_b$ are estimated online by the method developed in [29]. The $\mathbf{R}_z(\psi)$, $\mathbf{R}_y(\theta)$ and $\mathbf{R}_x(\phi) \in \mathfrak{SE}(3)$ are rotation matrixes:

$$\begin{aligned}
\mathbf{R}_z(\psi) &= \begin{bmatrix} \cos\psi & -\sin\psi & 0 \\ \sin\psi & \cos\psi & 0 \\ 0 & 0 & 1 \end{bmatrix} \\
\mathbf{R}_y(\theta) &= \begin{bmatrix} \cos\theta & 0 & \sin\theta \\ 0 & 1 & 0 \\ -\sin\theta & 0 & \cos\theta \end{bmatrix} \\
\mathbf{R}_x(\phi) &= \begin{bmatrix} 1 & 0 & 0 \\ 0 & \cos\phi & -\sin\phi \\ 0 & \sin\phi & \cos\phi \end{bmatrix}
\end{aligned} \tag{4.2}$$

4.1.2 UAV Dynamics and Kinematics

We denote the center of mass of UAV body in world frame by $\mathbf{r} \in \mathbb{R}^3$, then from Newton's law we have:

$$m\ddot{\mathbf{r}} = \begin{bmatrix} 0 \\ 0 \\ -mg \end{bmatrix} + {}^w\mathbf{R}_b \begin{bmatrix} 0 \\ 0 \\ \sum F_i \end{bmatrix} \tag{4.3}$$

where $m \in \mathbb{R}$ is the total weight of the UAV and $F_i \in \mathbb{R}$ is the lifting force provided by each motor. The components of the angular velocities of UAV in its body frame are denoted by p, q and $r \in \mathbb{R}$ and are related with θ, ϕ and $\psi \in \mathbb{R}$ by:

$$\begin{bmatrix} p \\ q \\ r \end{bmatrix} = \begin{bmatrix} \cos\theta & 0 & -\cos\phi\sin\theta \\ 0 & 1 & \sin\phi \\ \sin\theta & 0 & \cos\phi\cos\theta \end{bmatrix} \begin{bmatrix} \dot{\phi} \\ \dot{\theta} \\ \dot{\psi} \end{bmatrix} \quad (4.4)$$

In addition to force, each motor has also produced moment, $M_i \in \mathbb{R}$, perpendicular to $x_b - x_y$ plane. We denote the length from each motor to the center of mass by $L \in \mathbb{R}$ and the moment of inertia matrix along $x_b - y_b - z_b$ axes by $\mathbf{I} \in \mathbb{R}^{3 \times 3}$. We then have the following Euler equations:

$$\mathbf{I} \begin{bmatrix} \dot{p} \\ \dot{q} \\ \dot{r} \end{bmatrix} = \begin{bmatrix} L(F_2 - F_4) \\ L(F_3 - F_1) \\ M_1 - M_2 + M_3 - M_4 \end{bmatrix} - \begin{bmatrix} p \\ q \\ r \end{bmatrix} \times \mathbf{I} \begin{bmatrix} p \\ q \\ r \end{bmatrix} \quad (4.5)$$

As shown in Fig. 4.2, the control loops are divided into inner attitude control and outer position control. With the help of DJI Onboard SDK and owing to the differential flatness property, the state and input could be represented as algebraic functions of four carefully selected flat outputs $[r^T, \psi]$ and their derivatives [21]. This facilitates the generation of trajectories since any smooth trajectory (with reasonably bounded derivatives) in the space of flat outputs can be followed by the UAV. In Ch. 5.2, the main work of chaser UAV's motion planning goes to the design of the required trajectory.

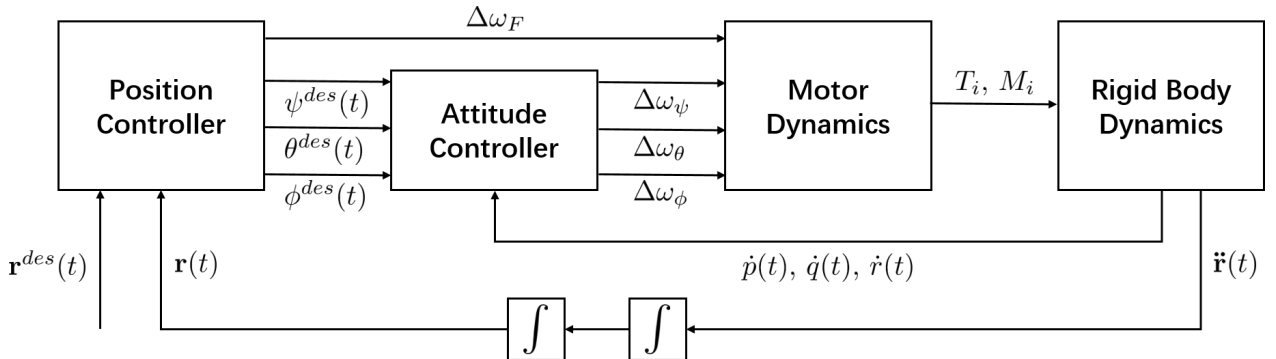


Figure 4.2. Nested control loops for position and attitude control, [22].

4.2 Hardware architecture

The hardware platform of our flocking system includes one follower UAV, one leader UAV and their remote controllers (RCs) as shown in Fig. 4.3 and Fig. 4.4. The leader UAV is fully manually controlled and the follower UAV is first controlled by the RC to take off, then the control authority is switched to the on-board mini computer and achieve autonomous driving. The RC is designed to have higher control authority than the on-board computer that human operator could prevent the UAV from fatal errors by switching control priority back to RC.

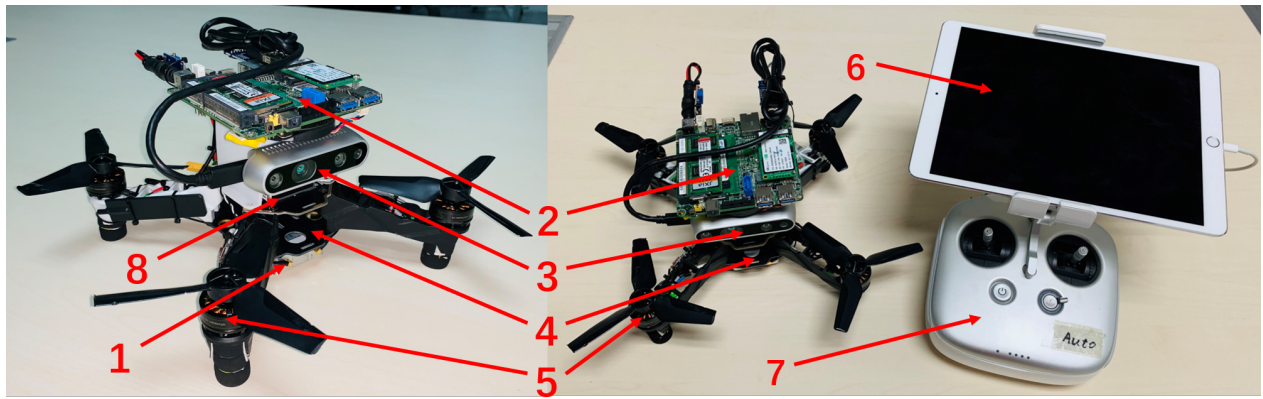
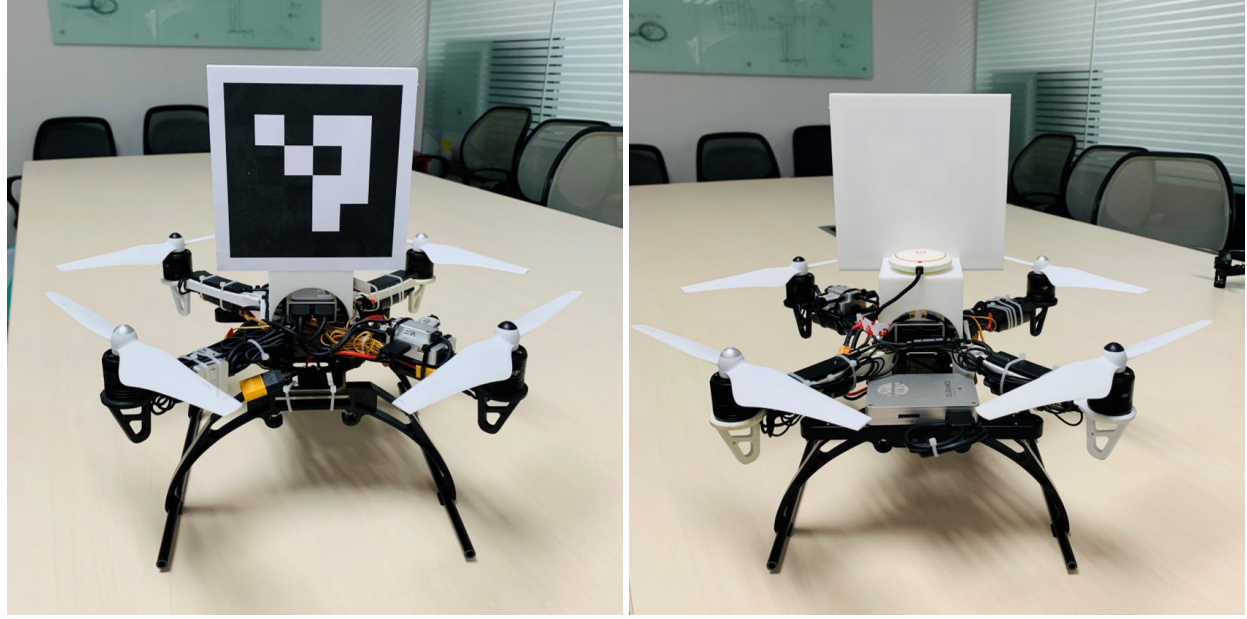


Figure 4.3. Follower UAV and remote controller panel: (1) Lightbridge 2 receiver; (2) Intel NUC mini computer; (3) Intel Realsense camera; (4) 4S LiPo Batter Case; (5) DJI snail motor; (6) iPad Live streaming panel; (7) DJI Lightbridge 2 remote controller; (8) DJI N3 flight controller.

Component	Weight(g)	Power(W)
Intel NUC i5 mini computer	125	15(avg)
Intel Realsense D435i camera	272	2.5(avg)
DJI N3 flight controller	92	3.3(avg)/5(peak)
DJI Lightbridge 2 receiver	70	7.8(avg)

Table 4.1. Weight and power consumption of components on the follower UAV.

The UAV frame consists of the mechanical construction, motors, propellers and the power supply module. Q250 is chosen as the follower UAV's frame for its compact size,



(a) Look from the back, with unique aruco code.

(b) Look from the front, with Guidance system mounted.

Figure 4.4. Leader UAV.

firm material and the flexibility in maneuvering in cluttered environment. DJI snail BLDC motors and 5-inch 3-blade propellers are mounted for their racing optimized propulsion system and rapid response time. 4S LiPo battery is selected for on-board power supply for its 16.8 V output, 4200 mAh capacity and rechargeable property. The detailed follower UAV's on-board power supply system is illustrated in Fig. 4.5. The total weight including the battery is 1.12 kg and the diagonal length is 25 cm. We use Intel NUC i5 mini computer as our follower UAV's on-board computing resource for both frontend processing and backend optimization (Ch. 5.2). We choose Intel Realsense Depth camera D435i as the forward looking camera for both perception and leader UAV feature recognition. It is outfitted with a stereo global shutter camera, with resolution up to 1920x1080 pixels, frame rate up to 90 FPS and direct depth map output. With sufficient tests, only the left monocular camera is employed to balance the power consumption. More details about on-board components can be found in Table 4.1.

The overall system stability is more emphasized than flexibility on leader UAV, where F330 frame with diagonal length of 33 cm, DJI 2312E BLDC motors, 7-inch propellers and the DJI Guidance vision-feedback position system are mounted. With Guidance system

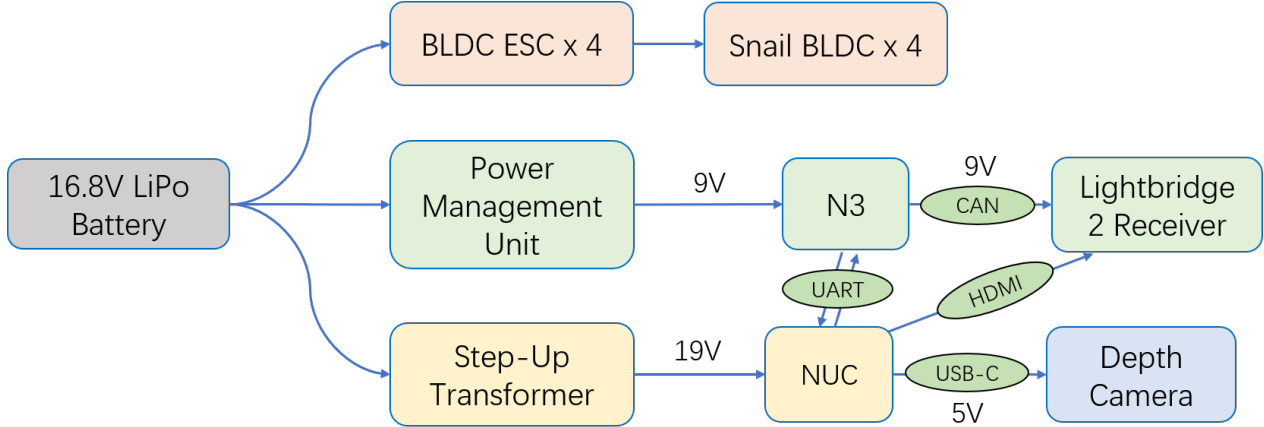


Figure 4.5. On-board power systems.

and its built-in ultrasonic sensor, it is easier for the leader UAV to hover and maneuver at a fixed height. The demand for computation and perception capability on leader UAV is lower than the follower, as its flight path is controlled by human operator, thus it is not embedded with any external processor. DJI N3 flight controllers are selected for both follower and leader UAVs, due to their high quality built-in IMU sensor and compatibility with DJI Lightbridge 2 for live streaming.

We choose to build two UAVs since our initial goal is to fill in the gap of the realization of flocking model on UAVs with distributed control algorithm and measurement method, and the field-of-view of one forward looking camera has limited the total number of UAVs. To extend the current setup to multiple UAVs, two fish-eye cameras (pointing forward-and-backward or left-and-right) or one omnidirectional camera (looking upward) are needed to cover wider FOVs, such that no blind point will exist in agents' perception system. Though these two UAVs differ in size and motor power, they all belong to quadrotors (Ch. 4.1) and their physical performances are very close that we consider them homogeneous and suitable for the realization of our flocking model (3.1, 3.2).

4.3 Software architecture

The software architecture is shown in Fig. 4.6. On the follower's mini i5 computer, 400 Hz IMU measurements and 30 Hz grey scale image data are fused in the visual-inertial state estimator [29] to obtain UAV self position and orientation. Unique aruco code [33] is

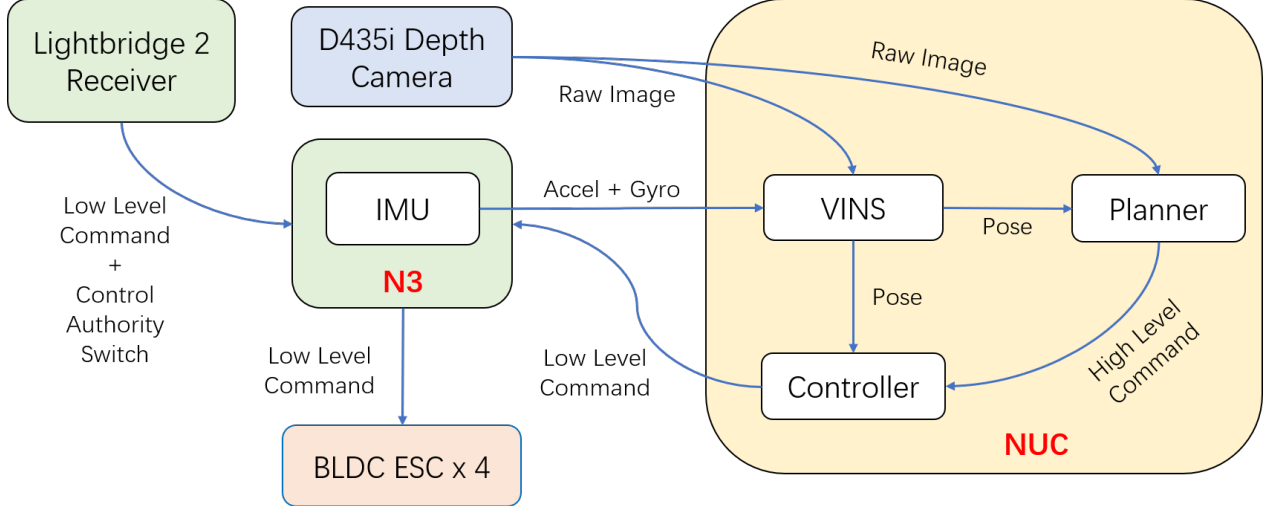


Figure 4.6. Software architecture.

attached on leader UAV to simplify the relative displacement and pose estimation. Unlike many existing flocking systems that rely on motion capture system (VICON), global positioning system (RTK) or LiDAR, our follower UAV only utilizes forward looking monocular camera for state estimation to maximally imitate natural birds. We show through both indoor and outdoor experiments that our minimal sensing setup is sufficient for the realization of our flocking model with Algorithm 1.

Algorithm 1 Flocking algorithm for the follower UAV.

```

1: if flocking signal triggered then
2:   obtain body pose estimation from VINS, capture leader's image;
3:   while new image do
4:     estimate relative displacement  $x_i - x_j$  (4.6);
5:     calculate relative velocity  $v_i - v_j$  from differentiation (4.8);
6:     calculate desired acceleration  $u_i$  from proposed model (3.1, 3.2);
7:     execute flocking command;
8:   end while
9: end if

```

The estimation of relative displacement $x_i - x_j$ is to estimate the translation ${}^c p_w$ from the world frame to the camera frame. In affine transformation (4.6), λ is a scaling factor, ${}^c R_w$ is the rotational matrix from the world frame to the camera frame, (u_c, v_c) and (x_w, y_w, z_w) denote the coordinates of the same one feature point (corners of the tag) in camera and world frames respectively, where (u_c, v_c) could be obtained from [33]. K denotes camera intrinsics which could be obtained from camera calibration. Since the real size ($l_{tag}=12$ cm) of the aruco tag is known, then 4 pairs of corresponding feature points

from two consecutive images are sufficient to estimate the ${}^c p_w$ [16].

$$\lambda \begin{bmatrix} u_c \\ v_c \\ 1 \end{bmatrix} = K \begin{bmatrix} I^{3 \times 3} & \mathbf{0}^{3 \times 1} \end{bmatrix} \begin{bmatrix} {}^c R_w & {}^c p_w \\ 0 & 1 \end{bmatrix} \begin{bmatrix} x_w \\ y_w \\ z_w \\ 1 \end{bmatrix} \quad (4.6)$$

$$K = \begin{bmatrix} f_x & 0 & u_0 \\ 0 & f_y & v_0 \\ 0 & 0 & 1 \end{bmatrix} \quad (4.7)$$

$$v_i(t) - v_j(t) = \frac{(x_i(t) - x_j(t)) - (x_i(t - \delta t) - x_j(t - \delta t))}{\delta t} \quad (4.8)$$

We have also utilized DJI Lightbridge 2 for remote debugging and monitoring (Fig. 4.3). The Lightbridge 2 transforms mini computer's desktop stream to iPad Pro for visualization, including current leader UAV's pose and live image processing output. This enables us to remotely manipulate the on-board computer while the UAV is in the air.

CHAPTER 5

EXPERIMENTS AND EVALUATION

In this section, we first present the performance of our proposed model in simulations and compare the results with the state-of-art models introduced in Ch. 2. We then realize the proposed method with our UAV flocking system and conduct real world experiments in both indoor and outdoor environments. We have also implemented a tracking algorithm with our system and compare their results in terms of flocking criteria.

5.1 Simulation of Flocking Models

We first show the influence of σ and β in (3.1) to the convergence of the flock in Fig. 5.1, where the averaged ψ_{angle} (1.1) of twenty simulation results are illustrated with three cases. The more ψ_{angle} gets close to one, the more convergent and aligned the flock is. As shown in the figure that the choice of σ has little impact on the convergence rate compared with β . When $\beta \leq \frac{1}{2}$, the convergence of the whole flock is unconditional which is coincident with our assumption in Ch. 3.1. We choose $\sigma = 1$ and $\beta = 0.25$ for all the following simulations and experiments. We compute the averaged results of ψ_{angle} and relative distance from twenty simulations and plot them in Fig. 5.2. We show that the cohesion, separation and alignment criteria still hold for our proposed model regardless of the number of total agents in the flock.

We compare our proposed flocking model with the ones in [42, 10, 8] in Ch. 2.1 with 2, 3 and 4 agents respectively. The initial positions are illustrated in Fig. 5.3 where the initial velocities are randomized. The positions of individual agents during the whole simulation are illustrated in Fig. 5.7 for reference. In Fig. 5.4 and Fig. 5.5, we show that our proposed model converge as fast as those in [42, 10, 8]. Especially, we show that the relative distance between neighboring agents in our proposed model is strictly bounded by the interval $(d_0^{\frac{1}{2}}, d_0^{\frac{1}{2}})$. Suppose certain minimum safety distance exists, such as $d_{\text{safe}} = 0.8$ in Fig. 5.6(b), our proposed model could successfully avoided collision with neighboring agents.

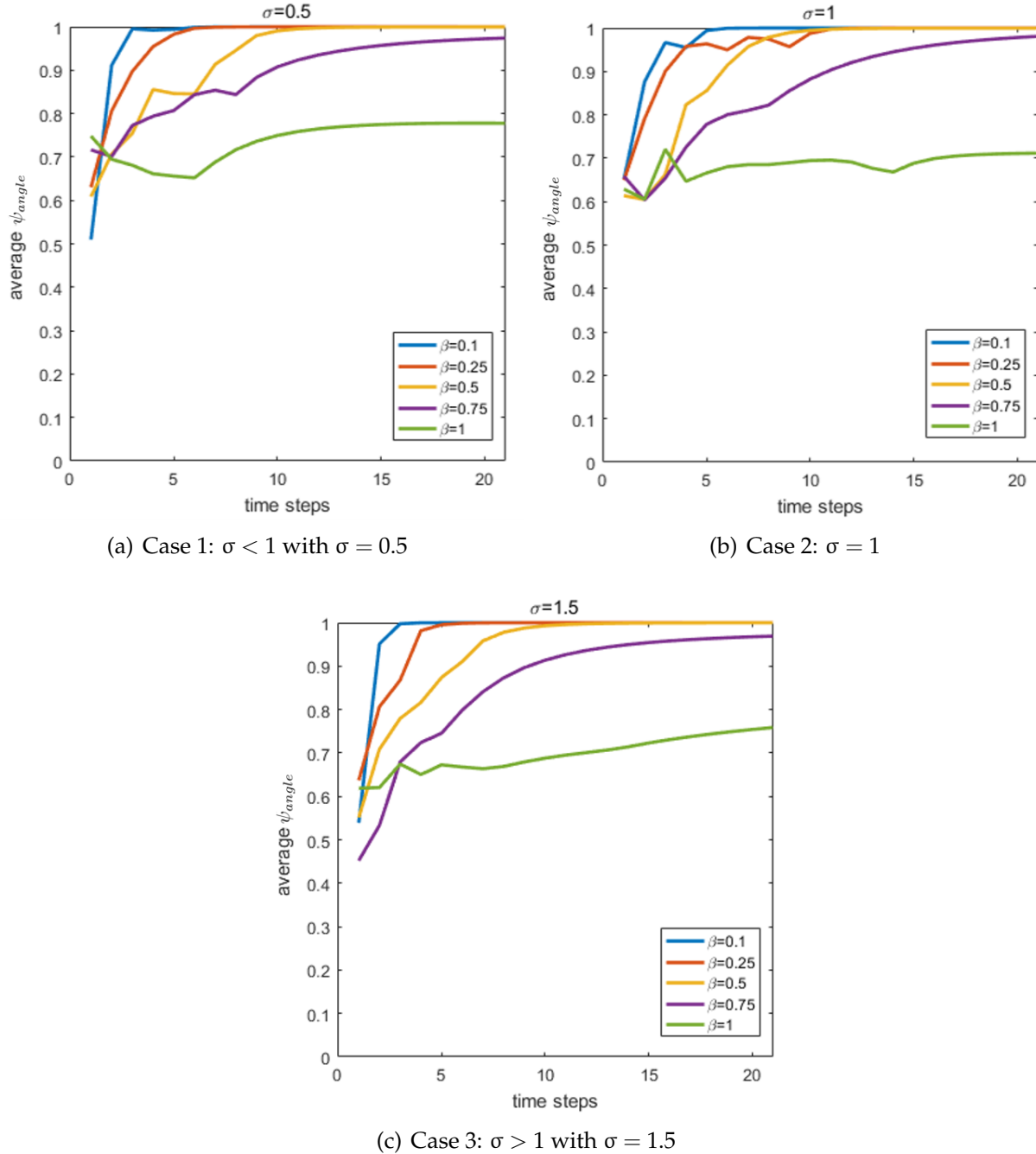


Figure 5.1. Averaged ψ_{angle} of twenty simulations of two agents w.r.t various σ, β . Their initial velocities are all randomized and nonzero.

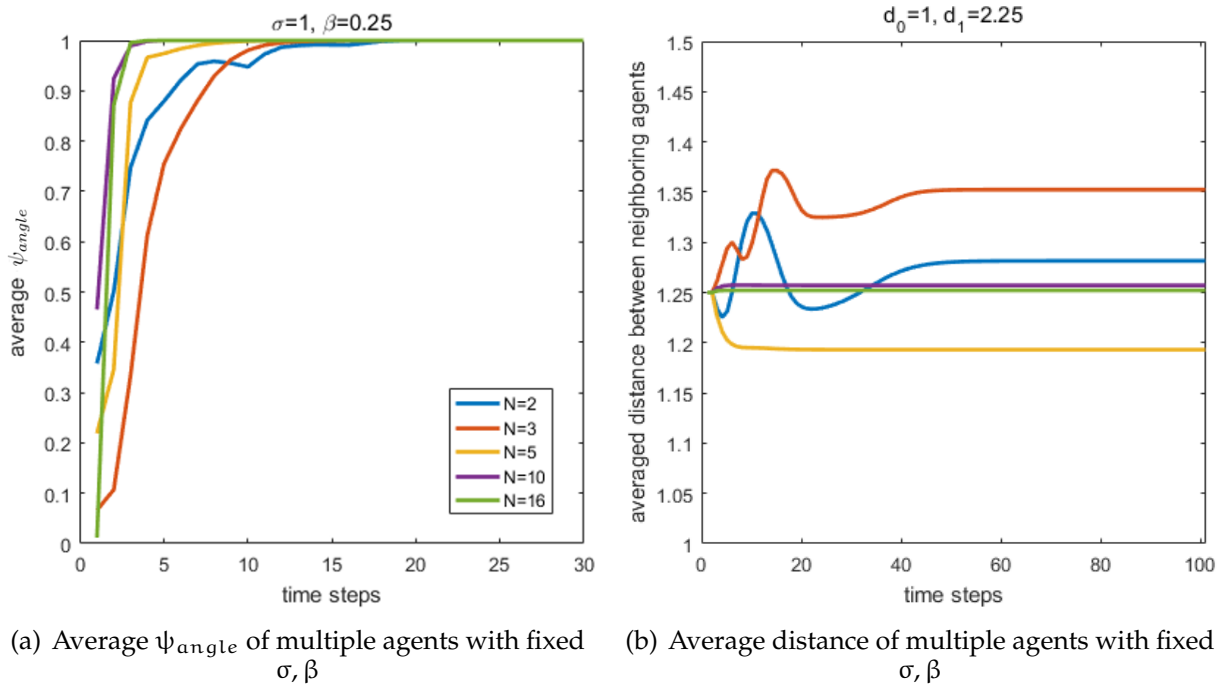


Figure 5.2. Average ψ_{angle} and relative distance of multiple agents with fixed $\sigma = 1$ and $\beta = 0.25$. Their initial velocity are all randomized and nonzero.

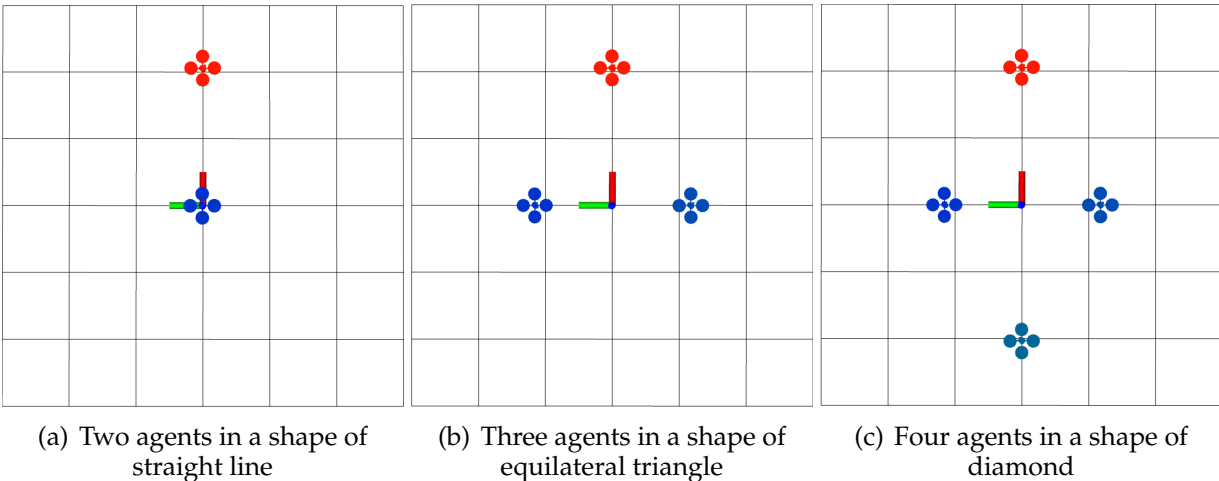


Figure 5.3. Initial position settings of multi-agent flocking simulations in MATLAB.

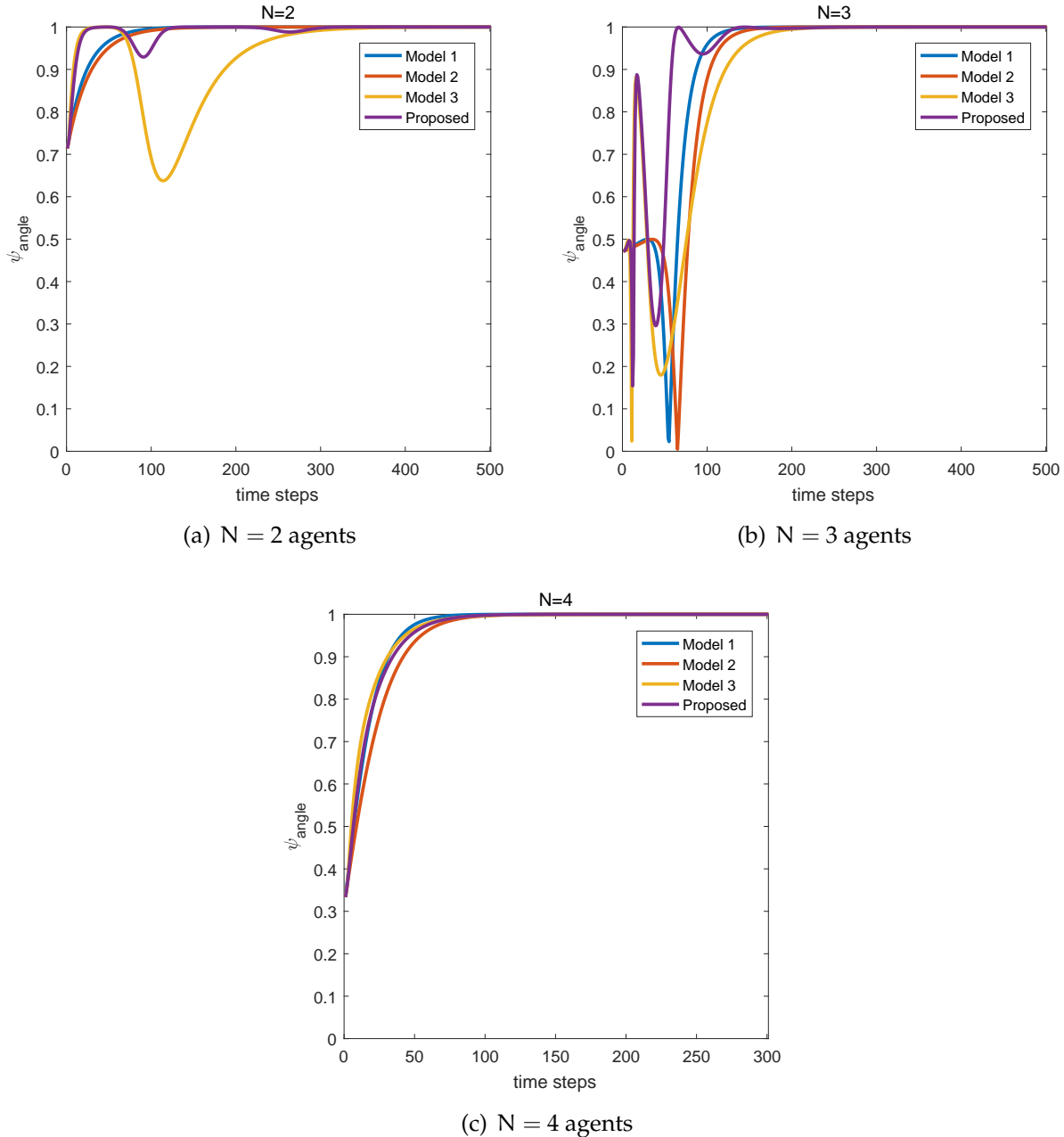


Figure 5.4. Convergence descriptors ψ_{angle} of model 1 ([42]), 2 ([10]), 3 ([8]) and our proposed one.

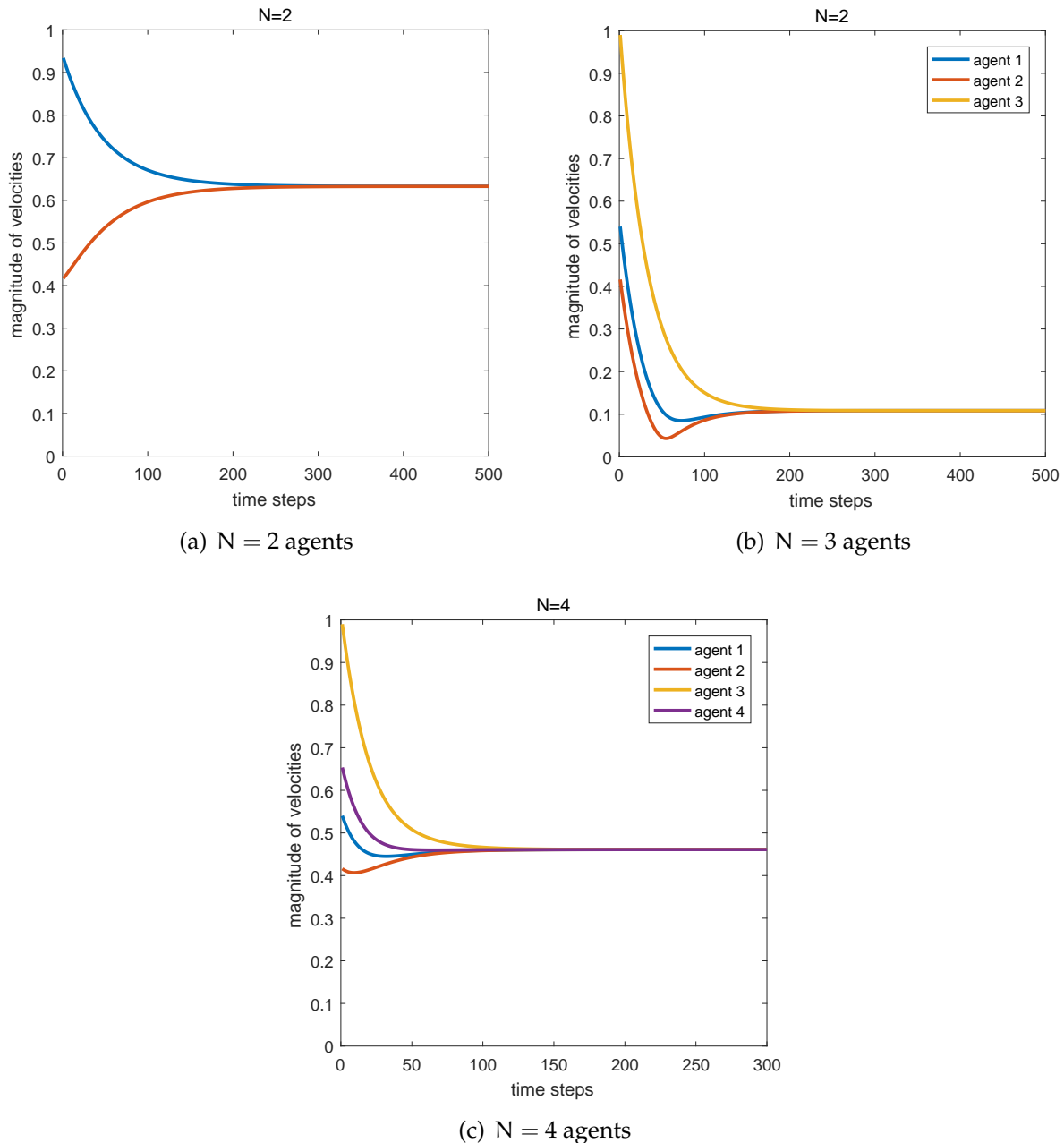


Figure 5.5. Magnitudes of agents' velocities of model 1 ([42]), 2 ([10]), 3 ([8]) and our proposed one.

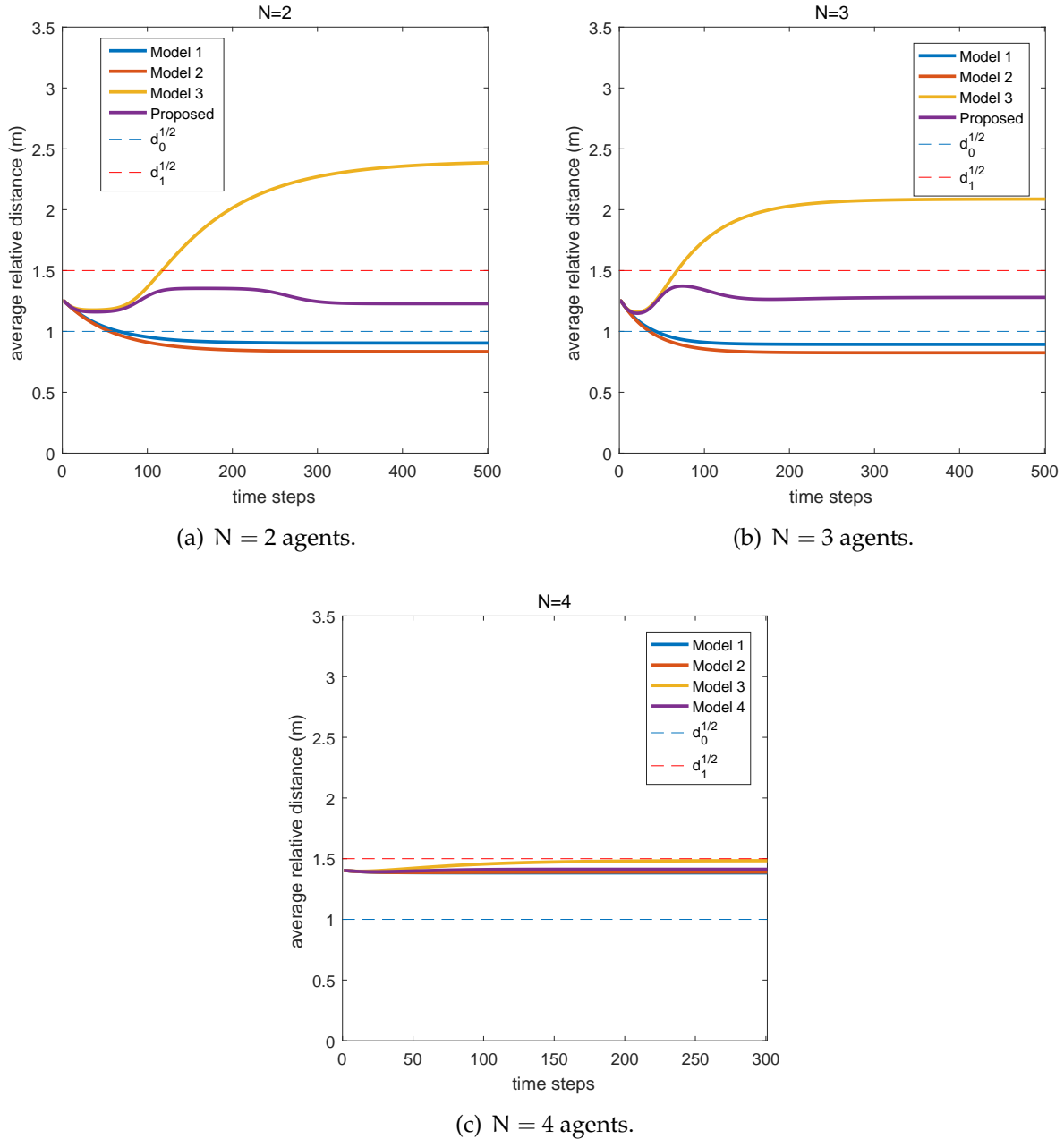
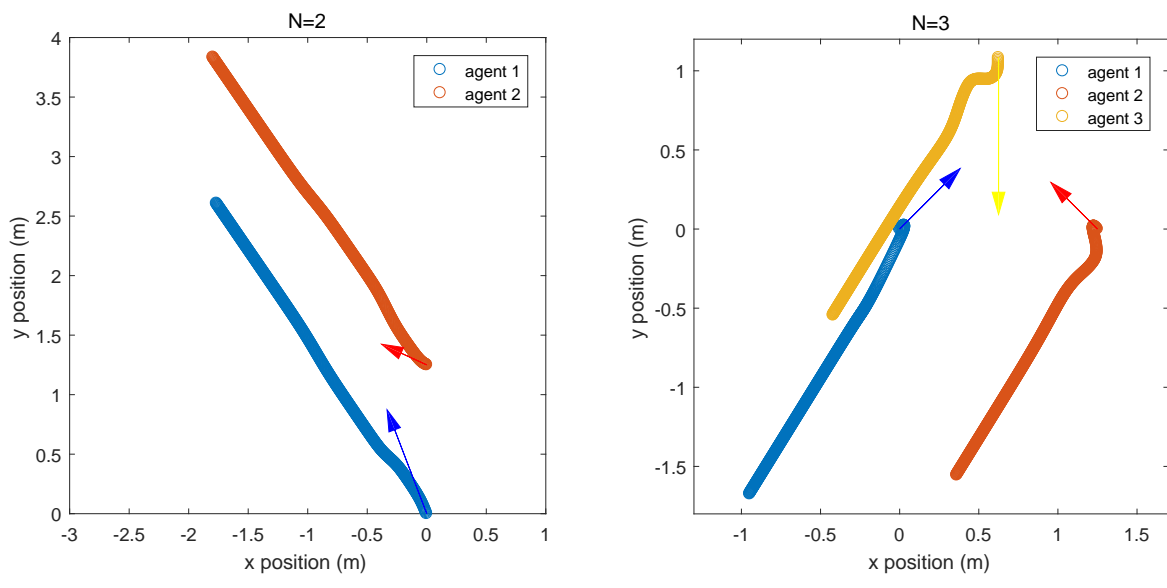
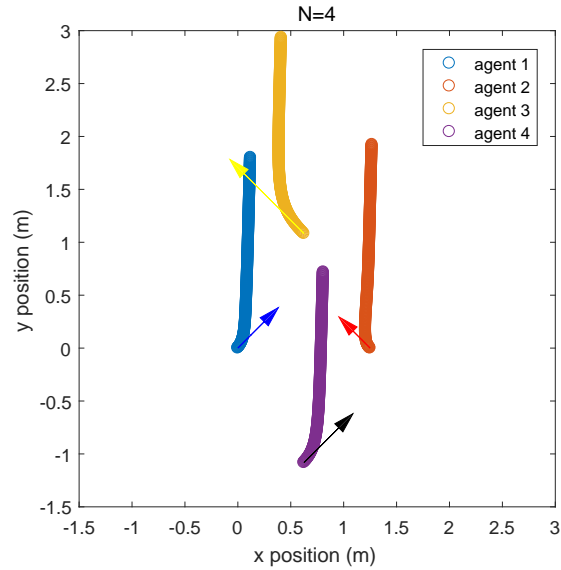


Figure 5.6. Average relative distances between neighboring agents. The blue and red dashed line indicate two boundaries ($d_0^{1/2}, d_1^{1/2}$) in our proposed model. Model 1, 2 and 3 are from [42], [10] and [8] respectively.



(a) $N = 2$ agents.

(b) $N = 3$ agents.



(c) $N = 4$ agents.

Figure 5.7. Motion simulations with initial velocities whose directions and magnitudes are indicated by corresponding arrows.

5.2 Comparison with Formation Algorithm

We have reproduced the formation algorithm (5.1, 5.2) in [6] and compared it with our flocking algorithm. The light green dots are the 3D positions of the leader calculated from captured images, a frame of which is shown in Fig. 5.8(b). As illustrated in Fig. 5.9, the formation algorithm has maintained the relative displacement between follower UAV and leader UAV, however, it is clearly seen in Fig. 5.9(a) that the delay is inevitable.

$$\min_{\hat{T}(\cdot)} \sum_{i=0}^L \|\hat{T}(t_i) - p_i\|_2^2 + \lambda_t \int_{t_l}^{t_m} \|\hat{T}^{(2)}(t)\|_2^2 dt \quad (5.1)$$

$$\min_{f(\cdot)} \int_{t_0}^{t_m} \|f(t) - T_s(t)\|_2^2 dt + \lambda_f \int_{t_0}^{t_m} \|f^{(3)}(t)\|_2^2 dt \quad (5.2)$$

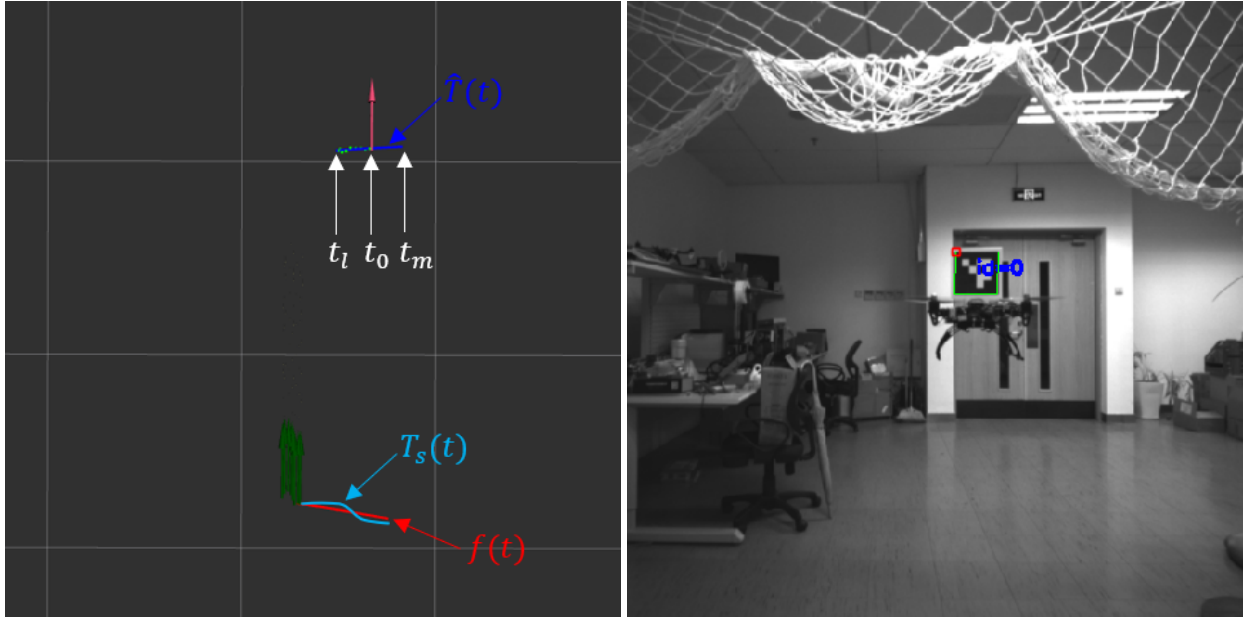


Figure 5.8. Formation algorithm in [6].

5.2.1 Formation Performance

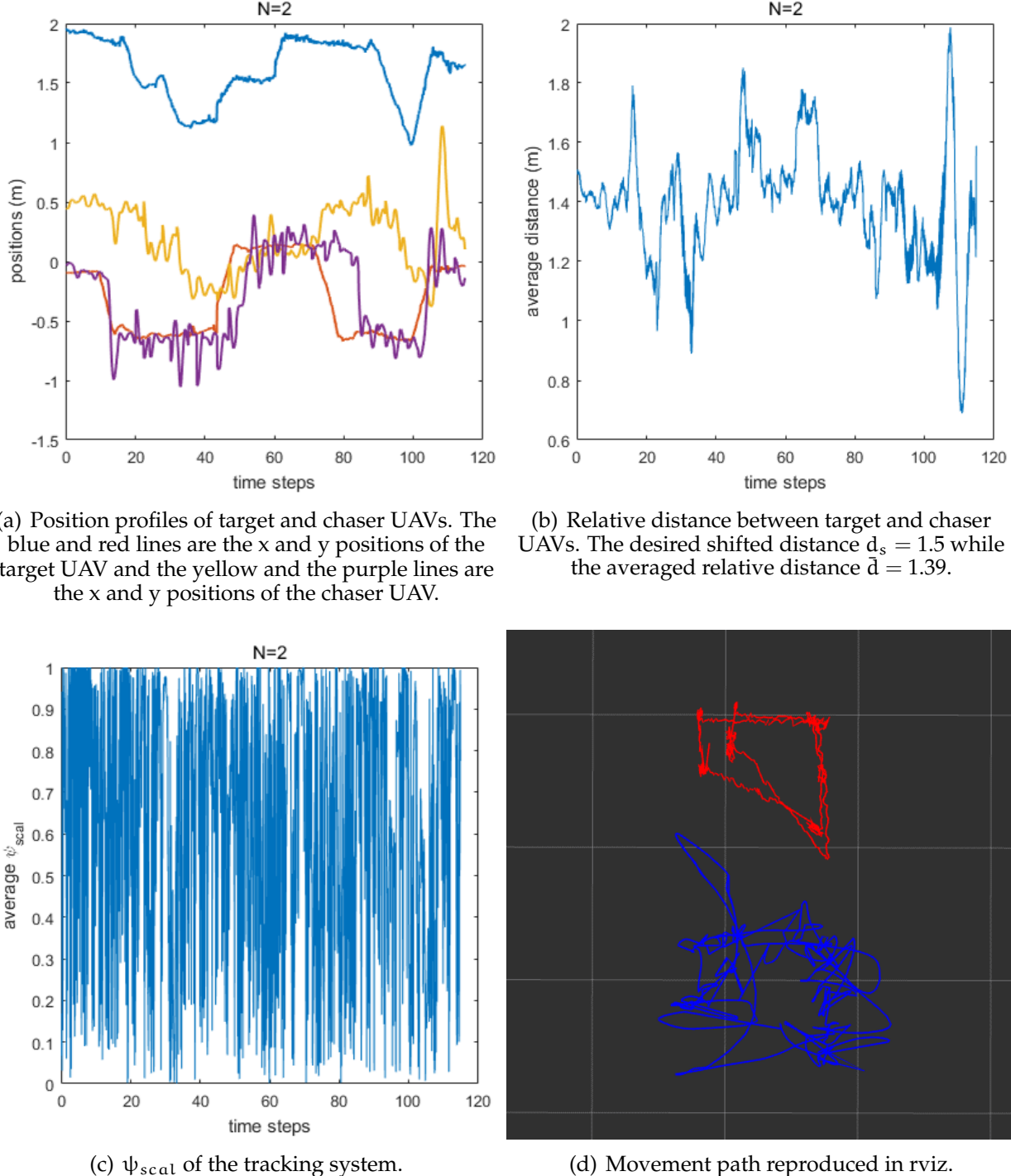


Figure 5.9. Plots of tracking algorithm.

5.3 Realization of Proposed Model

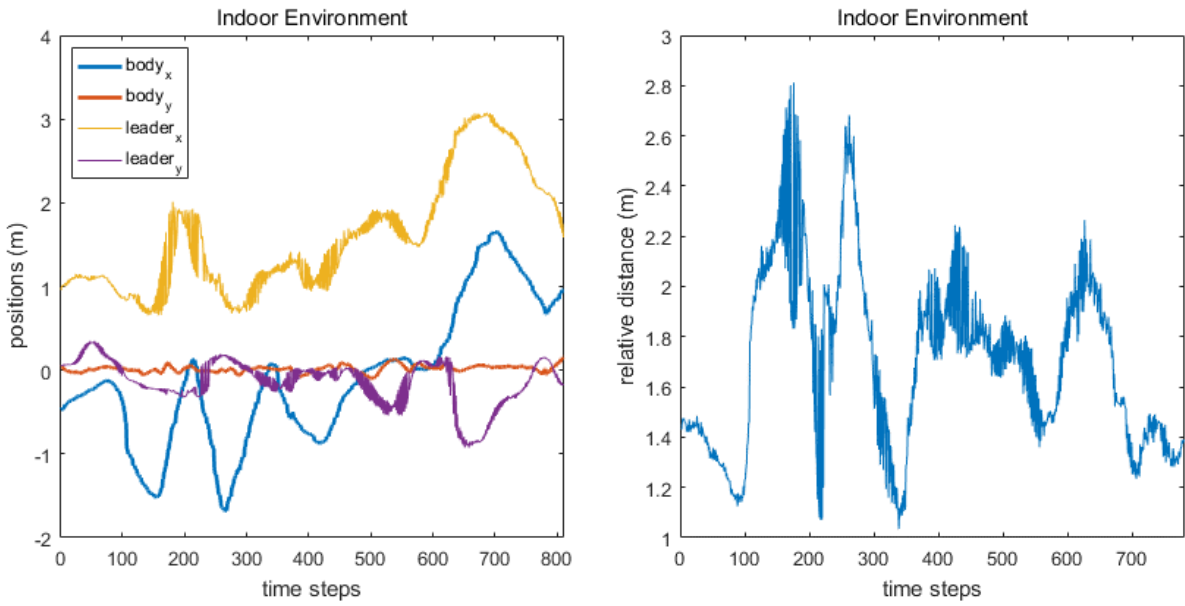
In this section, we demonstrate that our flocking system is able to operate in both indoor and outdoor GPS-denied environments. All the experiment settings are identical, where the follower UAV takes off first and hovers at desired height, waiting for the leader, then the leader UAV takes off and the control authority of follower switches to autonomous mode to begin flocking. The desired u_i is updated when a newer photo comes in and in each time interval (roughly 0.1 s) the latest u_i is being executed. The initial take off position of follower UAV is 1.5 m behind the leader UAV to match the requirement ($d_0 < \|x_i - x_j\|^2 < d_1$) with $d_0 = 1, d_1 = 8, K = 1, k = 2, \alpha = 1$ and $\beta = 0.25$ in Ch. 3.1. The maximum acceleration and velocity of follower UAV are set to $a_{max} = 2.5m/s^2$ and $v_{max} = 0.5m/s$ for safety reasons. In each experiment we show their position profile, relative distance, ψ_{angle} plot and their movement path reproduced in rviz. Due to the measurement noise, light condition and lack of ground truth, spikes appear randomly in all figures. We have shown that the trend of slope in ψ_{angle} plot is in accordance with that in position plot, the follower UAV is able stay flocking with the leader and the reaction of follower is rapid.

5.3.1 Indoor Environment

We have conducted two experiments in the indoor environment. We first let the leader UAV moves purely along the x-axis (positive pointing forward) and then y-axis (positive pointing left), with their results being illustrated in Fig. 5.10 and Fig. 5.11. Noted that ψ_{scal} plot is calculated with the data all obtained from follower UAV.

5.3.2 Outdoor Environment

In the outdoor environment, we let the leader UAV moves in the xy-plane. Due to the outdoor wind condition that the follower UAV has deviated a little from desired position, moreover, the relative distance between two UAVs is kept within the desired boundary.



(a) Position profiles of leader and follower UAVs.
The yellow and purple lines are the x and y positions of the leader UAV and the blue and the red lines are the x and y positions of the follower UAV.

(b) Relative distance between leader and follower UAVs in x axis.

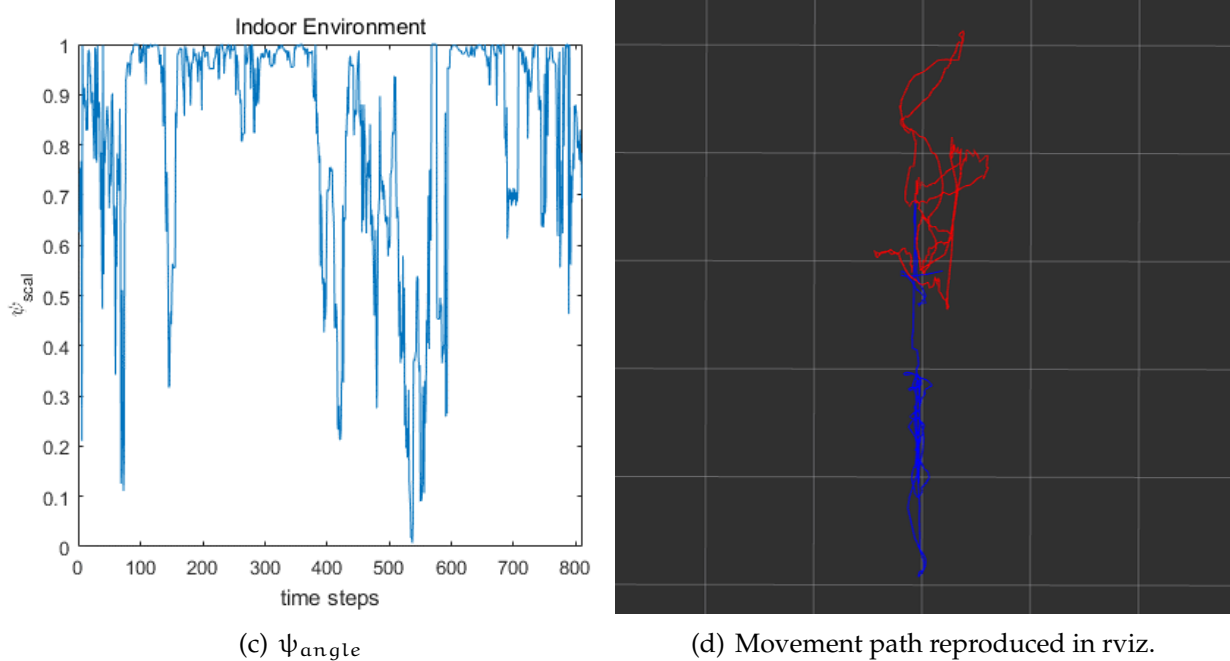


Figure 5.10. Flocking in x-axis.

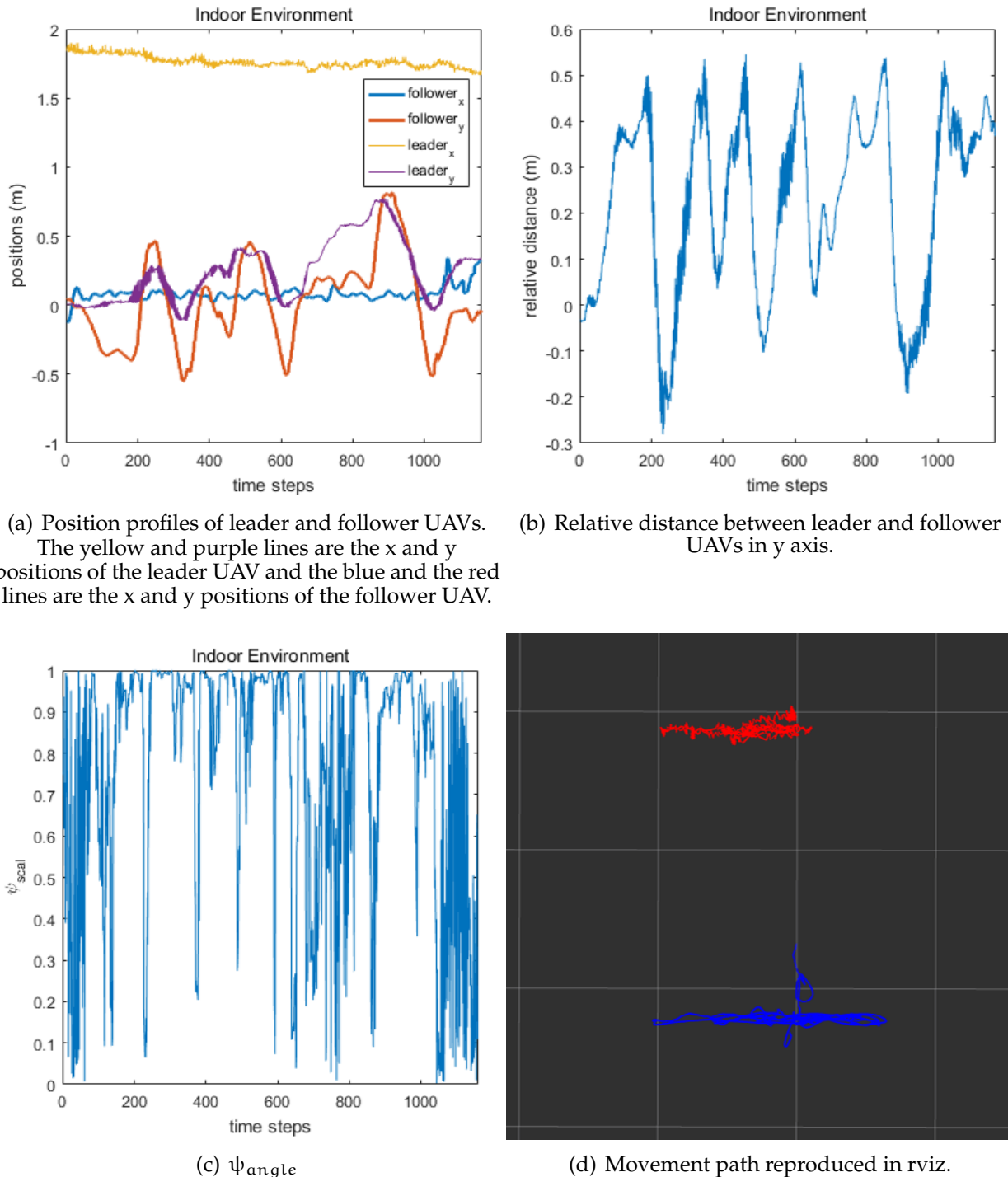


Figure 5.11. Flocking in y-axis.

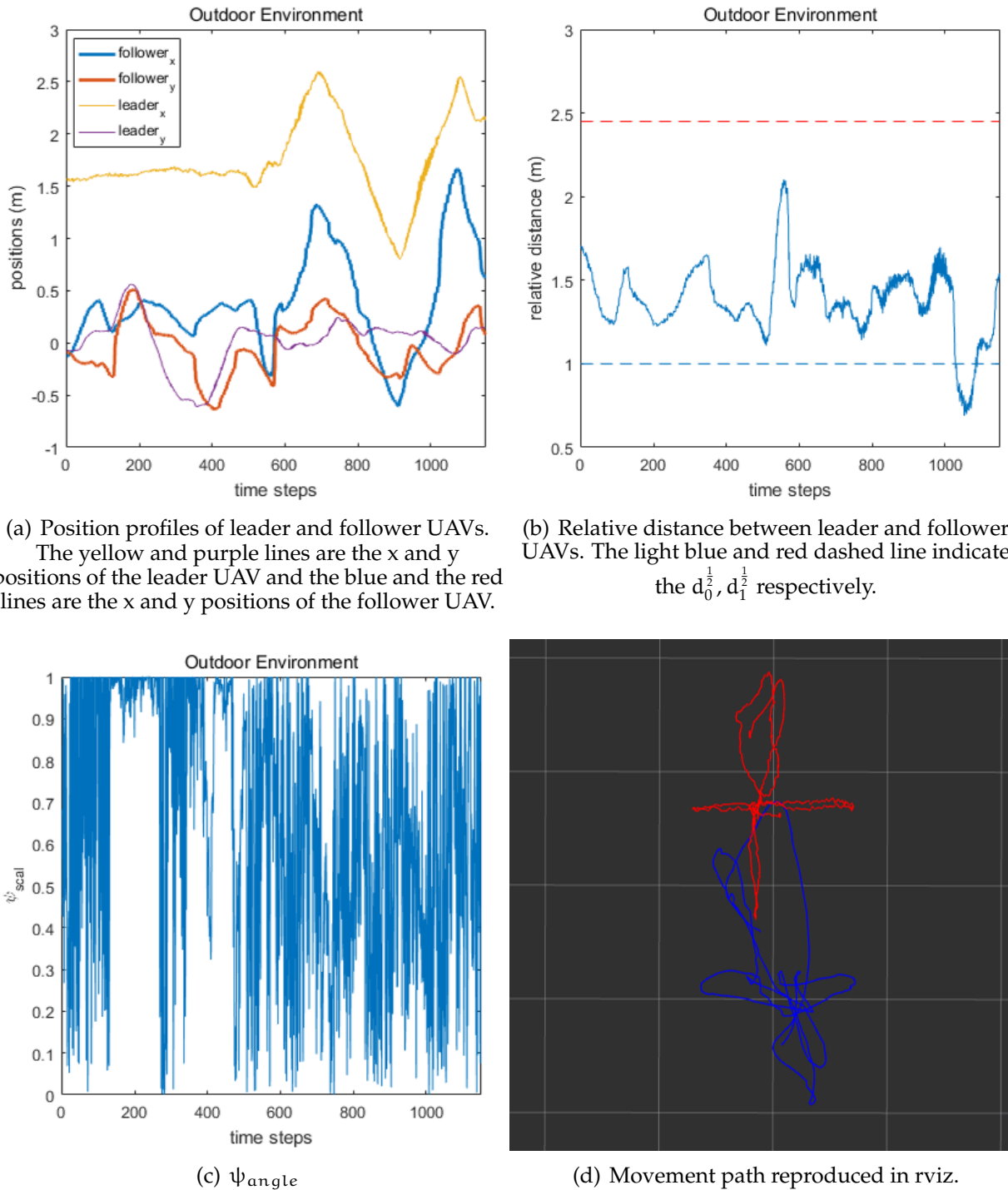


Figure 5.12. Flocking in xy-plane.

CHAPTER 6

CONCLUSION

In this thesis, a flocking system consisting two UAVs with our control law is presented and the detailed hardware and software architectures are introduced. The leader UAV is manually controlled and the follower UAV could be switched to autonomous mode and begins flocking with the leader. The monocular camera is used as the only on-board sensor for both follower UAV's state estimation and leader UAV's pose recognition. When in flocking, the follower UAV first percepts the surrounding environment to estimate self-state, then recognizes leader UAV's pose and calculates desired acceleration using our proposed model and third executes the desired input until next image is captured and processed.

Simulations, real world experiments and the comparison of the results from formation algorithm with our proposed method have been conducted and analysed. We have shown that our flocking system has met the three flocking criteria without relying on any external perception system or centralized control panel, achieved fast convergence rate and kept bounded relative distance with neighboring agents to avoid collision, given fine weather conditions.

Our future work will focus on the flocking of more than two quadrotors in GPS-denied environment, including extending our flocking model from fixed topology to dynamic topology, extending our flocking model form homogeneous to heterogeneous, introducing multiple fisheye cameras or an omnidirectional camera for perception and implementing ultra wide band (UWB) sensor for relative displacement measurement and internal communication.

REFERENCES

- [1] A. Askari, M. Mortazavi, and H. A. Talebi. Uav formation control via the virtual structure approach. *Journal of Aerospace Engineering*, 28(1):04014047, 2013.
- [2] T. Baca, G. Loianno, and M. Saska. Embedded model predictive control of unmanned micro aerial vehicles. In *International Conference on Methods and Models in Automation and Robotics (MMAR)*, pages 992–997. IEEE, 2016.
- [3] M. Ballerini, N. Cabibbo, R. Candelier, A. Cavagna, E. Cisbani, I. Giardina, V. Lecomte, A. Orlandi, G. Parisi, and A. Procaccini. Interaction ruling animal collective behavior depends on topological rather than metric distance: Evidence from a field study. *Proceedings of the national academy of sciences*, 105(4):1232–1237, 2008.
- [4] G. Beauchamp. Animal vigilance and group size: empirical findings. *Animal Vigilance*, pages 141–154, 2015.
- [5] D. Brandtner and M. Saska. Coherent swarming of unmanned micro aerial vehicles with minimum computational and communication requirements. In *European Conference on Mobile Robots (ECMR)*, pages 1–6. IEEE, 2017.
- [6] J. Chen, T. Liu, and S. Shen. Tracking a moving target in cluttered environments using a quadrotor. *IEEE/RSJ International Conference on Intelligent Robots and Systems (IROS)*, pages 446–453, 2016.
- [7] S. Chung, A. A. Paranjape, P. Dames, S. Shen, and V. Kumar. A survey on aerial swarm robotics. *IEEE Transactions on Robotics*, 34(4):837–855, 2018.
- [8] F. Cucker and J. Dong. Avoiding collisions in flocks. *IEEE Transactions on Automatic Control*, 55(5):1238–1243, 2010.
- [9] F. Cucker and J. Dong. On flocks influenced by closest neighbors. *Mathematical Models and Methods in Applied Sciences*, 26(14):2685–2708, 2016.
- [10] F. Cucker and S. Smale. Emergent behavior in flocks. *IEEE Transactions on automatic control*, 52(5):852–862, 2007.

- [11] M. A. Dehghani and M. B. Menhaj. Communication free leader–follower formation control of unmanned aircraft systems. *Robotics and Autonomous Systems*, 80:69–75, 2016.
- [12] D. V. Dimarogonas and K. J. Kyriakopoulos. Connectedness preserving distributed swarm aggregation for multiple kinematic robots. *IEEE Transactions on Robotics*, 24(5):1213–1223, 2008.
- [13] D. V. Dimarogonas and K. J. Kyriakopoulos. Inverse agreement protocols with application to distributed multi-agent dispersion. *IEEE Transactions on Automatic Control*, 54(3):657–663, 2009.
- [14] M. Dong and Z. Sun. A behavior-based architecture for unmanned aerial vehicles. In *Proceedings of the 2004 IEEE International Symposium on Intelligent Control*, pages 149–155. IEEE, 2004.
- [15] V. Gazi and K. M. Passino. Stability analysis of swarms. In *Proceedings of the 2002 American Control Conference*, volume 3, pages 1813–1818. IEEE, 2002.
- [16] R. I. Hartley and A. Zisserman. *Multiple view geometry in computer vision*. Cambridge University press, ISBN: 0521540518, second edition, 2004.
- [17] A. Jadbabaie, J. Lin, and A. S. Morse. Coordination of groups of mobile autonomous agents using nearest neighbor rules. *Departmental Papers (ESE)*, page 29, 2003.
- [18] R. A. Johnstone and D. J. D. Earn. Imperfect female choice and male mating skew on leks of different sizes. *Behavioral Ecology and Sociobiology*, 45(3-4):277–281, 1999.
- [19] N. E. Leonard and E. Fiorelli. Virtual leaders, artificial potentials and coordinated control of groups. In *Proceedings of the 40th IEEE Conference on Decision and Control*, volume 3, pages 2968–2973. IEEE, 2001.
- [20] S. Martin. Multi-agent flocking under topological interactions. *Systems & Control Letters*, 69:53–61, 2014.
- [21] D. Mellinger and V. Kumar. Minimum snap trajectory generation and control for quadrotors. In *IEEE International Conference on Robotics and Automation*, pages 2520–2525. IEEE, 2011.

- [22] N. Michael, D. Mellinger, Q. Lindsey, and V. Kumar. The grasp multiple micro-uav testbed. *IEEE Robotics & Automation Magazine*, 17(3):56–65, 2010.
- [23] L. Moreau. Stability of continuous-time distributed consensus algorithms. In *IEEE conference on decision and control (CDC)*, volume 4, pages 3998–4003. IEEE, 2004.
- [24] T. Nägeli, C. Conte, A. Domahidi, M. Morari, and O. Hilliges. Environment-independent formation flight for micro aerial vehicles. In *IEEE/RSJ International Conference on Intelligent Robots and Systems*, pages 1141–1146. IEEE, 2014.
- [25] R. Olfati-Saber. Flocking for multi-agent dynamic systems: Algorithms and theory. *IEEE Transactions on Automatic Control*, 51(3):401–420, 2006.
- [26] R. Olfati-Saber and R. M. Murray. Distributed cooperative control of multiple vehicle formations using structural potential functions. *IFAC Proceedings Volumes*, 35(1):495–500, 2002.
- [27] S. Omidshafiei, A. Agha-Mohammadi, C. Amato, and J. P. How. Decentralized control of partially observable markov decision processes using belief space macro-actions. In *IEEE International Conference on Robotics and Automation (ICRA)*, pages 5962–5969. IEEE, 2015.
- [28] T. J. Pitcher, A. E. Magurran, and I. J. Winfield. Fish in larger shoals find food faster. *Behavioral Ecology and Sociobiology*, 10(2):149–151, 1982.
- [29] T. Qin, P. Li, and S. Shen. Vins-mono: A robust and versatile monocular visual-inertial state estimator. *IEEE Transactions on Robotics*, 34(4):1004–1020, 2018.
- [30] W. Ren and R. W. Beard. Consensus seeking in multiagent systems under dynamically changing interaction topologies. *IEEE Transactions on automatic control*, 50(5):655–661, 2005.
- [31] W. Ren and N. Sorensen. Distributed coordination architecture for multi-robot formation control. *Robotics and Autonomous Systems*, 56(4):324–333, 2008.
- [32] C. W. Reynolds. *Flocks, herds and schools: A distributed behavioral model*, volume 21. ACM, 1987.

- [33] F. J. Romero-Ramirez, R. Muñoz-Salinas, and R. Medina-Carnicer. Speeded up detection of squared fiducial markers. *Image and vision Computing*, 76:38–47, 2018.
- [34] M. Saska, T. Baca, and D. Hert. Formations of unmanned micro aerial vehicles led by migrating virtual leader. In *International Conference on Control, Automation, Robotics and Vision (ICARCV)*, pages 1–6. IEEE, 2016.
- [35] M. Saska, J. Vakula, and L. Přeučil. Swarms of micro aerial vehicles stabilized under a visual relative localization. *IEEE International Conference on Robotics and Automation (ICRA)*, pages 3570–3575, 2014.
- [36] H. G. Tanner, A. Jadbabaie, and G. J. Pappas. Stable flocking of mobile agents, Part I: Fixed topology. In *IEEE International Conference on Decision and Control*, volume 2, pages 2010–2015. IEEE, 2003.
- [37] H. G. Tanner, A. Jadbabaie, and G. J. Pappas. Stable flocking of mobile agents Part II: Dynamic topology. In *IEEE International Conference on Decision and Control*, volume 2, pages 2016–2021. IEEE, 2003.
- [38] H. G. Tanner, A. Jadbabaie, and G. J. Pappas. Flocking in fixed and switching networks. *IEEE Transactions on Automatic control*, 52(5):863–868, 2007.
- [39] R. Tron, J. Thomas, G. Loianno, K. Daniilidis, and V. Kumar. Bearing-only formation control with auxiliary distance measurements, leaders, and collision avoidance. In *IEEE Conference on Decision and Control (CDC)*, pages 1806–1813. IEEE, 2016.
- [40] M. Turpin, N. Michael, and V. Kumar. Capt: Concurrent assignment and planning of trajectories for multiple robots. *The International Journal of Robotics Research*, 33(1):98–112, 2014.
- [41] G. Vásárhelyi, C. Virág, G. Somorjai, T. Nepusz, A. E. Eiben, and T. Vicsek. Optimized flocking of autonomous drones in confined environments. *Science Robotics*, 3(20):eaat3536, 2018.
- [42] T. Vicsek, A. Czirók, E. Ben-Jacob, I. Cohen, and Shochet. Novel type of phase transition in a system of self-driven particles. *Physical review letters*, 75(6):1226, 1995.

- [43] A. Weinstein, A. Cho, G. Loianno, and V. Kumar. Visual inertial odometry swarm: An autonomous swarm of vision-based quadrotors. *IEEE Robotics and Automation Letters*, 3(3):1801–1807, 2018.
- [44] T. Zhang. Unmanned aerial vehicle formation inspired by bird flocking and foraging behavior. *International Journal of Automation and Computing*, 15(4):402–416, 2018.